Correlations of Swine Internasal Suture Morphology and Mechanical Properties

by

Weerasinghe Mudiyanselage Kavya Sandeepanee Weerasinghe

A thesis submitted in partial fulfillment of the requirements for the degree of

Master of Science

Department of Mechanical Engineering

University of Alberta

Abstract

Bones in the skull are connected by craniofacial sutures, which are joints made of collagen fibers, vasculature, and an extracellular matrix. Sutures are straight and flexible at an organism's early ages and develop various morphological characteristics during growth. Patent (unfused) sutures respond to mechanical stimuli from activities such as mastication, locomotion, and intracranial pressure by changes to their morphology and material structure. The suture undergoes changes in morphology due to bone deposition and resorption at suture margins, as well as the formation of collagen fiber structure in the suture to resist stresses. The influence of morphological and material characteristics on the mechanical response of craniofacial sutures is crucial in understanding their growth and development.

In previous literature, when craniofacial sutures were modeled using finite element (FE) software, their complex three-dimensional (3D) morphology was simplified by taking measurements from only one plane in two dimensions (2D), typically the ectocranial or endocranial planes that are easily accessible from the cranial surfaces. Previous works that conducted mechanical experiments on craniofacial sutures, often took average values of suture morphological measurements across their 3D structure when finding correlations between morphology and mechanical properties. When making these simplifications during modeling, experiments, or statistical analysis, little explanation was given for the degree of impact on the results. Thus, this study is a step towards discovering the effect of the simplifications that are commonly used in literature.

This study can be divided into three stages. In the first stage, a mechanical experiment was conducted on fresh-frozen swine bone-suture-bone samples containing the internasal suture. Four to five samples were dissected from the maxilla of nine Duroc (female) juvenile swine. The test consisted of preloading and preconditioning followed by a quasi-static tensile test at a low strain regime. Low strain regimes were used to prevent any permanent deformation to the suture structure since the samples will be analyzed using micro-computed tomography (μCT) X-ray imaging to determine their morphological properties. In the mechanical experiment, the gradient of the load vs displacement data from the tensile loading stage was used as the mechanical property under investigation as a proxy for the suture stiffness.

In the second stage of the study, the width and interdigitation of the suture samples were obtained in 3D using μCT X-ray imaging. The first and second stages provided mechanical and morphological data for statistical analysis in the third stage. A multiple regression model was used to predict the stiffness of the suture samples. Internasal suture morphological data as well as the position of the sample in the maxilla and the thickness of the sample (measured as the length between the outer and inner surfaces of the nasal bone near the internasal suture), were used as independent variables.

Based on the mechanical test data, it was observed that the cranial sutures exhibit nonlinear behavior under loading. The nonlinear regions were likely caused by the materials that made up the suture such as the rearrangement of collagen fibers within the suture, which was observed at low loads. During tensile loading, the most significant factors affecting the gradient of load vs displacement data were found to be the mean suture width and the sample thickness. Further studies can investigate the effect of morphological

factors, such as suture interdigitations, on mechanical response under different loading conditions like bending and compression. Therefore, the mechanical behavior of sutures can be better understood by considering the morphological adaptations of sutures and depending on the loading condition applied to the suture, some suture morphological features might have more significance on their mechanical properties. Findings from this thesis will have potential implications on suture morphological factors to consider when modeling and conducting experiments on cranial sutures.

Preface

This work is an original work by W. M. Kavya Sandeepanee Weerasinghe. This study obtained a secondary use ethics exemption (reference number: ETR24, Project Name "Biomechanical testing of swine craniofacial tissues") from the University of Alberta Research Ethics Office. No part of this thesis has been previously published. The author was responsible for the data collection and analysis as well as the manuscript composition.

Acknowledgments

Table of Contents

List of Tables

List of Figures

List of Nomenclature and Acronyms

2D	Two Dimensional
3D	Three Dimensional
ANOVA	Analysis of Variance
LII	Linear Interdigitation Index
RSME	Root Mean Squared Error
SMRI	Surgical Medical Research Institute
µCT	Micro Computed Tomography
FE	Finite Element
l	Length
R	Correlation Coefficient in Regression Analysis
DM	Displacement Reached at the Maximum Load for a Preconditioning Cycle (mm)

Chapter 1: Introduction

1.1 Motivation

Craniofacial sutures are a network of connective tissues between bones of the skull. They are made up of an extracellular matrix, collagen fibers, vasculature, and various cell types such as those responsible for angiogenesis, osteogenesis, and formation of collagen fibers[1]. Craniofacial sutures are more compliant and can accommodate deformations compared to the surrounding bones, which have a higher stiffness and elastic modulus[1]. They also have important roles in shape formation and expansion of the skull during the growth of the organism and protecting the brain from minor shocks[1–3]. Additionally, sutures experience quasi-static loads from continuous loading due to growth, cyclic loading from mastication, locomotion, joint mobility, and muscle activity[2].

Investigation of sutures is crucial for the development of medical treatment methods, safety devices, and research related to the craniofacial region. For example, craniosynostosis is a medical condition that leads to the premature fusion of the sutures in the skull, found in infants, and affects one in 2000-2500 live births worldwide[4]. This can lead to an increase in cranial pressure, which can impact brain development, and lead to abnormal skull shapes, headaches, and visual and auditory impairments[4,5]. Thus, understanding the growth patterns of the craniofacial region is important to carry out medical interventions to treat abnormal conditions. In addition, orthodontic treatments such as rapid palatal expansion and reverse headgear application are common medical treatments that require the study of craniofacial suture response to mechanical loads[1].

Suture material properties, and their 2D/3D structure change throughout the life of an organism and show adaptations to their mechanical environment[6,7]. For example, pediatric human cranial bone was reported to be over 30 times stiffer than the coronal suture, while adult coronal sutures had similar properties to the bone and a low deformation before failure[8]. The suture mechanical environment changes with their location due to the functionality associated with each region of the skull[2,9]. For an example, skull bones

1

experience intracranial pressure from the expansion of the brain during development and maxillary bones mainly experience cyclic loading from mastication[2]. It has been shown that higher interdigitation was a suture adaptation to compression loading experienced during mastication in posterior internasal and nasofrontal sutures in miniature pigs[10]. In human craniofacial samples containing zygomaticotemporal, frontozygomatic, coronal and sagittal sutures, the bending strength was positively correlated to the sutural interdigitation, showing a possible adaptation to bending[11]. In addition, there are adaptations in mechanical properties due to sexual dimorphism. For example, male wild sheep show higher interdigitation for better stress transmission in the skull sutures than females due to head butting during fights between male animals[12]. Through various examples, it is clear that gaining insight into the mechanical behavior of sutures requires a comprehensive understanding of their morphological adaptations.

Sutures possess a complex geometry that plays a role in determining the mechanical behavior of the skull[11,13]. The morphology of sutures is influenced by a range of biological activities, including mastication, locomotion, and growth[1,10]. Consequently, several studies have attempted to investigate the extent to which morphological complexities affect the mechanical properties and stress distribution of the skull. For example, an increase in the suture volume between skull bones of goat was shown to increase energy absorption during impact loading[14]. The suture linear interdigitation index (LII) is a measurement of the suture's geometry. It is calculated as the ratio between the length of the path that the suture takes between the bones and the linear length between the beginning and endpoints of the suture in a 2D cross-section of the suture space (Equation 1). Figure 1 shows a μCT image of the internasal suture in a swine maxilla showing the suture path and linear length between its endpoints. In literature, it was discovered that strain energy in sutures decreases with decreasing LII[15], and bending strength increases with increasing LII[11]. The suture width is the distance between the opposite edges of a suture. It is also a commonly used morphological property. In one study, it was discovered that the suture width decreased when subjected to quasi-static compressive loading and increased when subjected to cyclic compressive loading[1].

$$LII\ (Linear\ Interdigitation\ Index) = \frac{l_{Suture\ Path\ Length}}{l_{Linear\ Suture\ Path}} \quad \text{Equation 1}$$
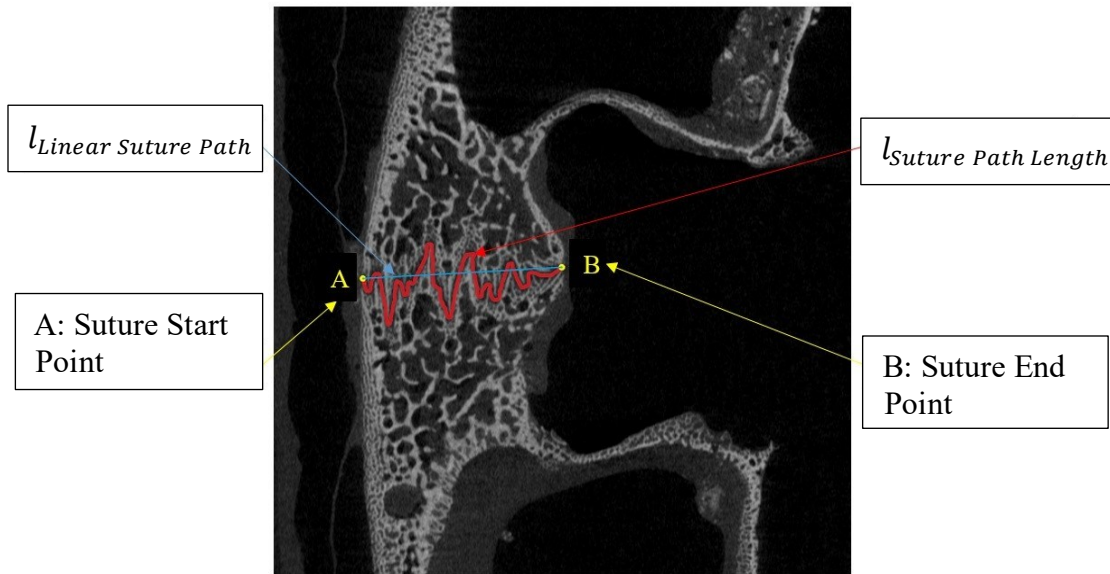
Figure 1: LII determination using suture path traced in red and linear length between suture start and end points in blue line

Suture LII and width describe suture geometry in 2D. Studies have typically used morphological measurements from a single plane, either ectocranial or endocranial, to represent the 3D structure of a suture[7,10,13]. In a study done on farm-bred swine, it has been shown that it is necessary to consider the 3D geometry of suture when investigating the mechanical response to loading[16]. Suture morphology can be taken in several cross-sectional sections through the thickness of the bone with the use of micro-computed tomography (μCT) X-ray imaging[16]. This method was also used in this thesis to evaluate the LII and the suture width through the 3D morphology of the suture.

Craniofacial sutures experience loading types such as quasi-static, cyclic, bending, and impact loads. Mechanical experiments conducted on sutures measured loading conditions such as in vivo cyclic loading through mastication[10,17–19], in vivo quasi-static loading due to growth[20], ex vivo low/ fast rate tensile/ compressive loading[21–23], and bending[14]. Studies have used parameters such as elastic modulus, to quantify mechanical properties of the skull. These studies attribute mechanical properties to various morphological characteristics such as LII, suture volume, or material properties such as collagen fiber

orientation. Since research studies deal with diverse types of sutures (e.g. location in the skull, type of organism, age) that have different morphological and material characteristics, it is difficult to utilize this information to model or predict the mechanical behavior of any given suture. Therefore, it is crucial to identify all variables, control factors, and limitations when investigating the mechanical behavior of sutures. Thus, although some studies suggest that the 3D morphology of craniofacial sutures may be important in their mechanical behavior, it is unclear which aspects of morphology play the most significant role in determining the mechanical response.

The focus of this thesis is to examine how the 3D geometry of sutures impacts their mechanical behavior. The high variability between different craniofacial sutures requires the consideration of multiple controlling factors. We focused on one type of suture from swine; internasal suture and applied quasi static tensile loading in low strain regimes. The internasal suture is between the nasal bones of the maxilla as shown in Figure 2. Multiple regression analysis was to develop a statistical model that predicted its mechanical properties by considering various 3D morphological measurements such as suture with and LII. A multiple regression model can use several independent variables and their relative contribution to predict the value of a single dependent variable[24]. Thus, this method was used in this thesis, to find the relative contribution of morphological properties such as suture width and LII in predicting the dependent variable, which is the gradient of load vs. displacement data from the mechanical experiment. This approach can help identify the degree to which morphological characteristics of the internasal suture contribute to its mechanical properties.
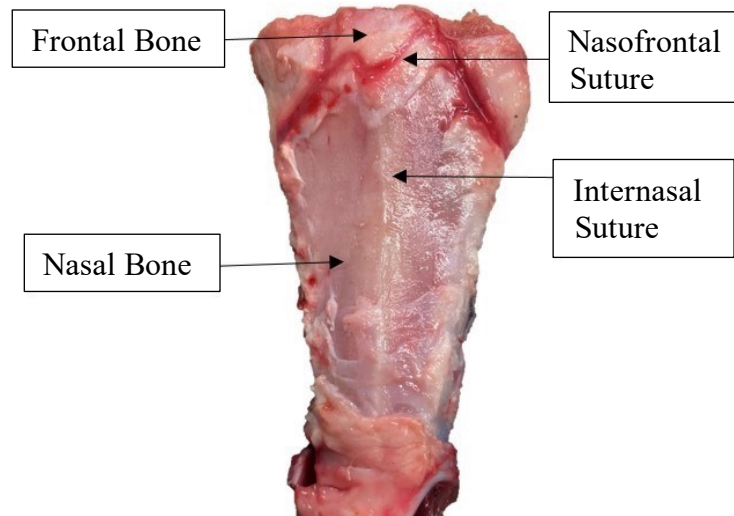
Figure 2: Anatomy of swine maxilla (top view)

1.2 Thesis Objectives

The objective of this thesis was to find correlations between morphological properties of the swine internasal suture and its mechanical properties under quasi static tensile loading. The objective was achieved through three main stages. The first stage focuses on investigating mechanical behavior of bone-suture-bone samples of the swine internasal suture using a mechanical experiment that applied quasi static tensile loading. The bone-suture-bone samples contained the nasal bone with internasal suture running in the middle. The experiment focuses on low-strain regimes where the sample has not yet transitioned into the failure region. The load vs. displacement data of all samples were analysed to obtain uniaxial stiffness, which was the mechanical property of interest.

In the second stage of the thesis, the 3D suture morphology is investigated utilizing μCT imaging techniques. The maxilla samples that were mechanically tested in the first stage were used for imaging. Previously developed methods to analyze suture μCT images were improved and adjusted to the specific needs of this thesis.

In the final stage of this thesis, a statistical analysis of the data obtained from previous steps was conducted. Multiple regression can be used to find statistical correlations between morphological data such as suture width and LII and the uniaxial stiffness of the

internasal suture samples. Findings of this study were used to explain the role of morphological factors for their mechanical response.

1.3 Thesis Contributions

This study is an exploration into the importance of craniofacial sutures when determining their mechanical behavior. With the use of ex vivo swine maxilla samples with mechanical tensile tests and μCT imaging, this study gathered information on the mechanical properties and the 3D morphological geometry of the internasal suture that runs between the nasal bones. The use of a multiple regression model allowed for a statistical analysis of the relationship between morphological properties and mechanical response. By assessing the degree of contribution of each morphological property, it was possible to gain a practical understanding of the morphological properties that govern the material behavior under tensile loading.

The information obtained from the statistical model can be used to optimize skull models built using finite element modeling. If one or more morphological data have a strong statistical correlation with the mechanical properties, this might mean that they are directly influenced by each other in their functional environment in the organism. Thus, this study contributes to obtaining a deeper understanding of the role of the craniofacial sutures in the skull.

1.4 Thesis Outline

This thesis contains four chapters. Chapter 2 is a comprehensive literature review of the suture material composition, suture morphology, imaging techniques, and mechanical testing methods. It can be used to understand the research done so far and the research gap that needs to be addressed.

Chapter 3 is the main thesis work including the experiment design, μCT imaging, and the determination of the statistical model. It also discusses the results and the conclusions from the experimental data.

Chapter 4 is a discussion of the future work that can be built upon the findings of this thesis and the limitations of all the methods.

Appendix A included all the physical measurements of all the dissected samples. Appendix B shows all the load vs displacement data separated by maxilla and the linear regression run on these data to obtain uniaxial stiffness, which was used as the mechanical property in multiple regression. Appendix C provides the MATLAB scripts used in μCT image analysis. Appendix D is a detailed summary of the morphological results obtained in μCT imaging.

Chapter 2: Literature Review

2.1 Craniofacial Suture Material Composition

Craniofacial sutures are a network of soft tissues between the bones of the skull. Sutures are composite structures, with collagen fibers, extracellular matrix, various cell types, and vasculature being the most prominent materials[1]. Craniofacial sutures act as joints in the skull, with viscoelastic material properties, which undergo quasistatic strain, and cyclic loading, and absorb small impact forces[25,26]. The viscoelastic nature of sutures is due to the rearrangement and deformation of collagen fibers, displacement/flow of water and other fluids, and stress relaxation due to the interaction between these components[23].

Every craniofacial suture has a unique composition because of the ability to respond to its unique functional environment[1,2]. Mechanotransduction is a biological process that transforms mechanical stresses to signals that respond to them and help sutures adapt their material composition[27]. Suture borders contain mesenchymal stem cells, which form osteoblasts which are responsible for the process of bone formation, also known as osteogenesis[28]. Additionally, sutures contain osteocytes that aid in bone remodeling in response to mechanical loading, and osteoclasts that are responsible for bone resorption[16,26]. The central area of the suture mesenchyme consists of fibroblasts, and mesenchymal stem cells. Fibroblasts are responsible for the production of collagen fibers in the suture[26]. Thus, it is evident that the structure and material composition of cranial sutures are continuously altered by various cell types.

Craniofacial sutures are flexible, thick, and straight during early stages of development [29]. They assist in passing the skull through the birth canal due to their low stiffness and flexibility[29]. They also aid expansion of the skull due to the enlargement of the brain during development[29]. With age, sutures develop a more complex collagen fiber structure and variable amounts of suture interdigitation, due to mechanotransduction. Some braincase sutures fuse with maturity, but facial sutures remain patent (unfused) and support more deformation and large biting forces[18].

It is known that the collagen fibers in the suture enable flexibility and deformation. Thus, a suitable arrangement of collagen fibers can help suture withstand tension, compression, and shear loading[30]. Various imaging techniques have been used to find the collagen fiber structure, orientation, and different cell types and their locations in the suture. For example, light microscopy has been used to reveal the areas of sutures with tension and compression-resisting fiber arrangements[23]. Another instance of light microscopy shows obliquely arranged fibers that resist compression[10]. Additionally, histology, pathological methods, and synchrotron X-ray microtomography have been used in literature to study suture material composition[2,10,25]. Collagen fibers in sutures were predicted to have a fan-like shape in a previous study, with more fibers attached to convex regions of suture morphology where bone deposition occurs[25]. These regions experience higher levels of tensile stress. In the same study, this fan-like pattern was observed in adult mice skull sutures using synchrotron X-ray microtomography[25]. It has been shown in literature that sagittal sutures of mice contain osteogenic fronts, which are regions of advancing bone formation[31]. These fronts create convex-shaped areas, while concave regions are areas of bone resorption and retreating bone. These regions were reported to result in higher interdigitations and adaptations that can withstand compressive loading environments[31].

2.2 Craniofacial Suture Morphology

Suture morphology has been shown in previous studies to influence the mechanical behavior of sutures, including stress distribution, stiffness, bending strength, and energy absorption during strain[10,30]. During the early stages of development, cranial sutures have a straight and less interdigitated geometry[32,33]. As growth progresses, sutures experience loading from higher masticatory, locomotion, and growth activities[1,2]. Due to cell activity that is associated with mechanotransduction, as discussed in the previous section[32,33], the 3D geometry of these sutures transforms and creates 3D morphological adaptations for their functional environment[1,25]. Experimental studies have been done to observe these adaptations. For example, it was reported that the sutures of miniature pigs with well-developed interdigitations were associated with a compressive mechanical environment while, sutures with fewer interdigitations were areas of tension[10,17]. Suture interdigitations provide a higher surface area between the two bones of the skull and provide areas for

9

collagen fiber attachment that resist compression and tensile strains[10]. Moreover, cranial sutures can absorb more energy than bone in impact loading, and higher interdigitations increase the spatial volume between the bones and contribute to higher energy absorption in the skull[14,30]. A previous study summarized the various adaptations sutures undergo due to different strain regimes[1]. The same study observed morphological changes, such as wider suture width due to cyclic loading, and tensile quasi static loading. Compressive quasi static loading was shown to reduce suture width and increase interdigitation[1].

Studies have been done to observe morphological adaptations numerically and using finite element (FE) modeling. In a mathematical model that described the suture morphological formation, it was observed that osteogenic cells migrate to the suture margins and contribute to bone deposition that forms convex structures, known as interdigitations[25]. Another mathematical model that aimed to predict the formation of suture interdigitations and the maintenance of suture thickness using the molecular interactions in the suture[32]. This model was built by observing the changes to suture interdigitation of mice from 3-8 weeks using µCT scanning, and these changes were described using a mathematical model that included osteogenic differentiation and substrate molecule contraction as two main factors that changed the suture interdigitation[32]. The model considered concentration and diffusion of mesenchymal cells that produced substrate molecules which promoted osteogenesis in the cranial suture. This model was shown to explain how interdigitations of sutures adapt to mechanical loads using their molecular activity[32].

FE models of sutures often simplify their morphologies by measuring their LII and suture width in one 2D plane, typically ectocranial or endo cranial surfaces of the skull bone, and do not consider the 3D complexity[15,30,34]. Previous studies have shown correlations between morphology and material properties through FE models. For example, several models of bone-suture-bone structures with idealized suture material properties such as isotropic and orthotropic properties have examined the effect of interdigitation and reported that suture strain energy generally decreases as LII increases under uniaxial loading[15,34]. These studies used a sinusoidal pattern and a constant suture width through the length of the suture to represent their morphology[15,34]. However, the implications of

10

simplifying morphology are still not well understood and not explained in literature. Full skull FE models of swine, extant fish and mice used μCT imaging techniques to better represent the complex geometry of suture models, but their accuracy was affected by the mesh quality, idealized material properties applied (e.g. isotropic), loading scenario, boundary conditions, and the number of models used in the study[34–37]. Therefore, it is crucial to understand the effects of simplifying the morphology and to verify the results with experimental methods when building suture models that can efficiently and accurately predict their behavior.

Often suture morphology is described numerically in 2D in previous literature. Suture width and LII are commonly used parameters that have been used to quantify suture complexity[10,16]. Images of ectocranial and endocranial sections have been used to represent the suture geometry and take measurements of interdigitation and width for the entire 3D geometry[7,10,38]. There were studies that considered suture geometry as a sinusoidal wave with varying dimensions for each tooth as shown in Figure 3[39,40]. This method used parameters such as sinuosity index, and morphological irregularity using tooth wavelength (λ), tooth tip angle (θ), and amplitude (A) (Figure 3). The apparent fact that sutures do not follow a perfect sinusoidal pattern and have other geometries makes using these parameters difficult. 3D μCT imaging has been used previously in FE modeling to get a more accurate structure of the skull sutures[16,36,38]. μCT imaging was used in a previous study to analyze suture 2D geometry in a plane and its variability in 3D using several 2D planes across the thickness of the skull bone[16]. The method included finding LII and suture width to quantify the suture morphology. This method used by Remesz et al, was modified to analyse the μCT imaging of internasal sutures and derive their morphological properties in this thesis. Additionally, Remesz et al[16] conducted an FE analysis on the effect of suture morphology on their mechanical properties under tensile loading. It has been shown that while a 2D geometry may be sufficient for determining bulk mechanical properties, an increase in suture complexity results in larger variations between the maximum, minimum, and average values of these properties[16]. When conducting a study, the morphological properties considered should correspond to the complexity of each suture and the mechanical properties of interest.
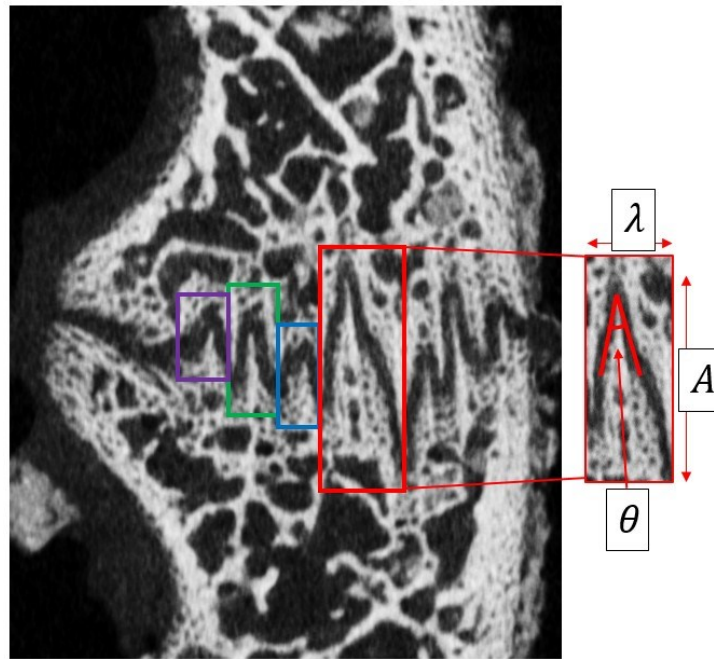
Figure 3: Sinusoidal wave method used in literature[39] for quantifying suture morphology showing 4 tooth units in the geometry separated by each box. parameters used to measure each tooth include wavelength (λ), tooth tip angle (θ), and amplitude (a), shown for one tooth unit in red box

Swine craniofacial sutures such as the nasofrontal, internasal and zygomatico-squamosal sutures have been commonly used in literature for mechanical testing[16]. In this thesis, internasal suture of swine was used due to the ease of access in the maxillary region during dissection. The internasal suture from miniature pigs was reported to be in compression in vivo during mastication and typically sutures under compression has been shown to adapt by having higher interdigitations than those under tension[16]. In literature, it was observed to be a straight suture that appears to have an LII of approximately 1 from the sagittal view but has higher interdigitation through the thickness of the bone, in the coronal view (Figure 4). The coronal plane of the internasal suture from miniature pigs had approximately LII of 1.8-3.4, the highest LII observed from the mid-region of the maxilla [16]. The internasal suture can be evaluated only in the coronal view, as the LII in the sagittal view remains approximately one consistently throughout the skull bone thickness. This will simplify the need to consider the sagittal plan when evaluating the morphology.
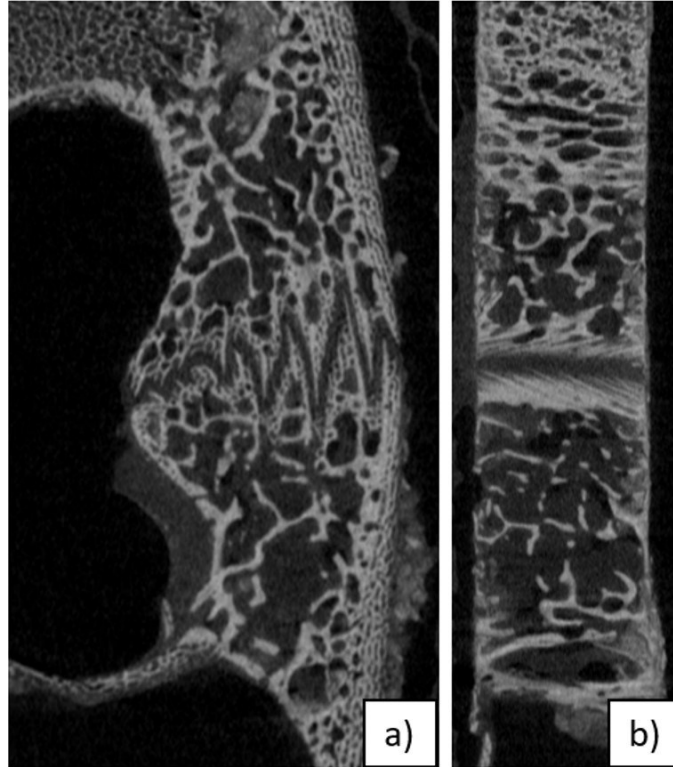
Figure 4: µCT image from a sample a) coronal view (with high LII) b) sagittal view (LII approximately 1)

2.3 Craniofacial Suture Mechanical Analysis

Previous studies have used in vivo [10,17–20] and ex vivo[21–23] methods to determine the mechanical behavior of sutures. Bone-suture-bone samples that consist of the suture sandwiched between two cranial bones are often dissected from the skull to apply loading conditions such as compression, tension, cyclic, quasi static and bending[8,21–23,41]. In a previous study, bone-suture-bone samples of human zygomaticotemporal, frontozygomatic, coronal and sagittal sutures were tested in bending to show that bending strength and LII are positively correlated[11]. In another study, tensile and compressive loading at slow (similar to suture growth rate) and fast (similar to mastication) rates were applied to swine nasofrontal bone-suture-bone samples[23]. It has been shown that the loading rate had little effect on their mechanical properties and the samples had higher elastic moduli in tension than in compression[23]. The viscoelastic mechanical behavior of bone-suture-bone samples from neonatal rats was reported by applying tensile loading to

13

failure and identifying various regions such as initial toe region, followed by a high increase in load and finally failure region[22]. Mechanical properties such as stiffness (load/displacement), ultimate stress and elastic modulus were used to describe mechanical properties in literature[22,23]. Through previous studies, it is evident that ex vivo craniofacial samples containing bone and suture are often used to understand their mechanical behavior of cranial sutures.

Human cranial bone samples with sagittal and coronal sutures were reported to have lower elastic modulus and ultimate stress but higher ultimate strain compared to cranial parietal and frontal bone samples without sutures[42]. The high elastic modulus of bones makes them more resistant to deformation than unfused sutures, which are more flexible and deformable[1]. When a load is applied to the skull, the sutures bear the brunt of the deformation since the suture was often found to be much less stiff than the bone[1,8]. In a previous study the peak strain at failure of tensile loading for nasal bone of swine was 260-320 $\mu\varepsilon$, while the peak strain of nasofrontal suture was 5300-9400 $\mu\varepsilon$[23]. In the same study it was reported that at failure, the peak stress in the tensile loading test for nasal bones was 1-1.2 MPa, while for nasofrontal suture, it was 0.8-1.5 MPa[23]. Thus, bones in the skull typically have a much higher resistance to loads and deformation than sutures[15]. Therefore, the deformation caused by loading is mostly due to the sutures. However, as sutures undergo the process of maturation, they increase in patency due to bone ossification, which ultimately leads to a higher level of elastic modulus and stiffness[18,23,43]. In the human skull, the metopic suture completely fuses by the second year of life, and the sagittal, coronal, squamosal, and lambdoid sutures close during the fourth and fifth decades of life[44]. In contrast, facial sutures were found to remain unfused for longer[18,23]. Thus, the mechanical response of cranial sutures to loading will be influenced by their age[43].

Additionally, cranial suture mechanical properties will be affected by several other factors, including the morphological, geometrical, and physiological characteristics of the suture and bone, and the type and rate of loading applied during the experiment to the specimen[21,45]. When measuring the mechanical properties of bone-suture-bone samples, it is crucial to consider the specimen's geometry. A study that conducted tensile tests on sagittal sutures in rats, calculated the sutural stiffness by performing linear regression on

force-displacement data points[21]. Stiffness per length was derived by dividing the stiffness by the sample length[21]. Sutural stress was calculated by dividing the tensile force by the cross-sectional area (sample width × sample Length) and the strain was the displacement divided by the suture width of the sample (Figure 5)[21]. During dissection, studies often control for specimen width and length, allowing for comparison in mechanical behavior between samples[22,23]. Therefore, while evaluating suture mechanical properties, it is essential to consider the sample's geometry as it can significantly influence the suture material in the bone-suture-bone sample.
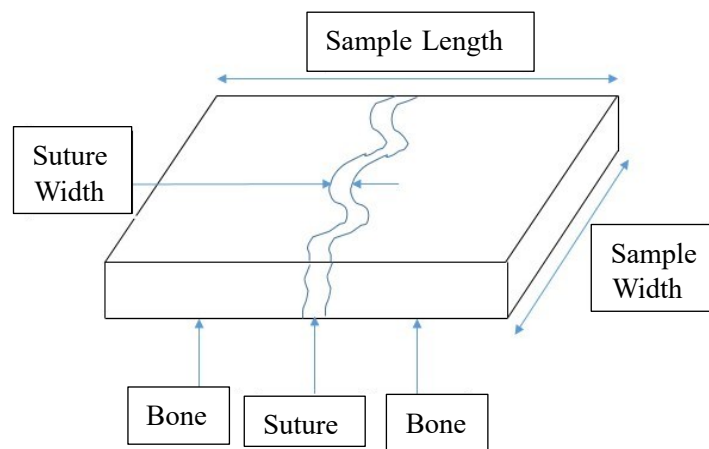
Figure 5: Measurement of a bone-suture-bone sample, suture width (W), sample length (l), sample width (SW)

Previous studies have been conducted to determine the mechanical behavior of the skull based solely on the mechanical properties of the cranial bone[45,46]. The cranial bone is a sandwich-like structure composed of dense bone on the outer layers and a porous lattice structure on the interior. The bone's porous structure has high energy-absorbing properties, and the sandwich structure has high stiffness and bending strength[46–48]. Human adult cranial bone samples were used to find that their material properties were affected by load rate and sample position in the skull[48]. When determining the mechanical properties of the skull, cranial sutures are shown to be crucial as they have widely different material and mechanical properties than the bone. For example, when rat skull models in FE included the suture their local strain magnitudes and stress distributions were affected, and sutures

played an important functional role by distribution forces during mastication and brain growth across the skull[49].

Statistical methods such as simple linear regression, and multiple regression were used to compare suture morphological characteristics to mechanical behavior in literature. Linear regression was used for human cadaver samples to show that the bending strength increases significantly with increasing interdigitation index[11]. Pearson correlation coefficient (r) was used to report correlation between higher interdigitation and compressive loading at the nasofrontal suture during mastication in swine craniofacial sutures[10]. Additionally, multiple regression was used in cranial samples of goats to show the significance of age and suture interdigitation on energy absorption and bending strength[14]. In the same study, it was found that for internasal sutures of goats, age was not a significant predictor of either energy absorption or bending strength at high or low loading rates, but suture interdigitation was significant in bending. As the suture interdigitation increases, the suture material joining two bones in the skull increases[14]. This results in an increase in the number of collagen fiber connections, which aids in higher energy absorption[14]. In addition, the interdigitations physically interlock, increasing resistance to bending strength[14]. Linear regression and correlation coefficients such as Pearson's r have been used frequently to find the correlation between one mechanical property and one morphological property[10,11,20,50]. Multiple regression was less frequently used[14], but it can utilize multiple independent variables to predict a mechanical property.

Despite previous studies on the mechanical behavior of cranial sutures and their correlation with morphology, it remains unclear which morphological factors have the greatest impact on resulting mechanical properties. Understanding the correlations between craniofacial suture morphology and mechnical properties can help identify the effects of commonly used simplification in suture FE models such as using suture measurements from only one 2D plane[15,30,34], using averages of suture width and LII[10,16], and using sinusoidal patters to represent geometry[30]. Multiple regression allows to use several independent variables in the same statistical model to find their relative contributions in predicting the value of a single dependent variable[24]. This method can be used to determine

which suture morphological properties need to be included and which simplifications have the least impact on a mechanical property to obtain a more accurate FE model.

Chapter 3: Correlations of Cranial Suture Morphology and Mechanics

3.1 Introduction

Craniofacial sutures are fibrous connective tissues that join the bones of the skull[2]. Compared to the surrounding skull bones that have a higher ultimate stress and elastic modulus, craniofacial sutures exhibit lower elastic modulus, stiffness, and ultimate strain values[1,42]. Due to their mechanical properties, the suture network between the bones is an integral part of the skull as it facilitates deformation and energy absorption[1,14,51,52]. Energy absorption properties of craniofacial sutures assist in traumatic events such as sudden impact forces, and head butting/fighting for animals[1,2,12]. Sutures also facilitate everyday activities such as mastication and locomotion[1,2,17,20]. Due to the functional role of craniofacial sutures, studies have focused on understanding their mechanical environment, morphology, and material composition[10,14,22,23,35,49,53,54].

Craniofacial sutures are a composite structure mainly containing collagen fibers, extracellular matrix, and vasculature[1,10]. They have viscoelastic and anisotropic material properties due to their composition[1,54,55]. Additionally, craniofacial sutures are areas of growth in the skull due to the various cell types that promote bone and suture formation[1,4]. For example, osteocytic cells are present at bone fronts and they contribute to bone growth[26]. Fibrocytic cells present at the mid-region of the suture are responsible for the formation of fibers in the extracellular matrix[16,26]. The variety of cells present regulates the morphology and material properties of sutures, and they change with location and functional environment[16,26].

Craniofacial sutures are straight and less stiff at an early age of development[1]. During birth, the sutures need to be flexible for the skull to exit the birth canal. As the brain and sensory organs (optic, auditory, gustatory, and olfactory) expand in the skull, they are areas of growth and help shape the cranium and facial region during development. As sutures mature, they adapt to their functional environment as they experience loading conditions

such as tension, compression, shear, and bending forces from daily activities such as mastication and locomotion, as well as quasi-static loading from intracranial pressure[1,32]. Previous literature shows evidence that suture bone growth fronts are affected by such mechanical stimuli[56,57]. In a study on the changes in suture growth and morphology of miniature pigs, the posterior interfrontal suture was reported to be in compression during mastication for 3-month-old pigs and they were highly interdigitated with oblique fibers[20]. In older pigs, the posterior interfrontal suture strain decreased in magnitude and underwent compression and tension. The morphology of the suture changed, and it was interdigitated endocranially but butt-ended ectocranially showing possible adaptations to loading conditions[20]. In another study involving miniature pigs, the collagen fibers in the internasal suture were arranged to resist compression, and interfrontal sutures were arranged to resist tension[10]. This indicated that the material composition of the suture is arranged according to its functional environment. Thus, it is clear that craniofacial sutures have morphological characteristics that are variable through the skull thickness, location in the skull, age, and mechanical environment.

Studies have explored the effect of complex 2D/3D variability of suture structures on their mechanical behavior with FE models. In one study exploring the mechanical role of cranial sutures of the rat skull, they used μCT to develop a 3D model of the cranium with and without the sutures. They discovered that the inclusion of sutures is important in the local strain patterns at various parts of the skull during feeding instead of the overall strain regime[36,49]. It was reported that the addition of sutures to pig skull models changed the strain patterns, orientations, and magnitudes of the skull[36]. These studies show that sutures affect the mechanical environment of various regions of the skull, such as the maxilla, mandible, and cranium because these regions have different functional environments. Further, FE models of sutures with different suture geometries that resulted in the same LII had varying overall strains to failure, which suggests that the local geometries of sutures might also affect their bulk mechanical behavior[39]. Another study that utilized μCT scanning evaluated the mechanical response of a suture with 3D complexity of the suture with FE models to determine the importance of morphology if the local mechanics are of interest[16]. The same study considered differences in FE modes that considered only 2D

sections such as ectocranial, endocranial, and mid planes and 3D models that used 3D μCT morphology[16]. FE models that only considered one 2D section for the entire suture morphology had different minimum and maximum stress/strain results than those with 3D complex morphology under tensile load[16]. Thus, studies using a sinusoidal pattern or a single plane from the suture to represent the suture throughout the thickness of the skull might oversimplify the complex morphology of the skull since it affects their local/bulk mechanical responses[34,39]. When modeling sutures, it is also common practice to simplify their complex morphometry and viscoelastic material properties[11,15,35]. The mechanical behavior of sutures under various loading conditions and with complex 3D structures is not well understood due to these simplifications made in previous studies. Therefore, it is essential to identify the morphological and material properties of sutures that have the most significant impact on their mechanical behavior.

Furthermore, the application of stresses and strains experimentally to bone-suture-bone samples is a frequently used method to investigate the mechanical properties of craniofacial sutures. A study that used tensile tests on cranial suture specimens of Wistar rats revealed the non-linear nature of the mechanical behavior to rupture consisting of an initial toe region, and rapid increase in tensile load until failure region[22]. Tensile and compression tests on pig nasofrontal sutures also revealed an initial toe region, elastic region, and failure region[23]. Studies have examined the effects of external forces on bone-suture-bone samples and have discovered links between their structure and mechanical properties[14,21,22,41]. However, it is uncertain which morphological factors play a significant role in determining the mechanical characteristics of sutures under varying loading conditions. To gain a better understanding, it is necessary to consider the 3D complex geometry of the suture as well as the impact of each morphological factor on its mechanical properties. This will enable us to identify the effect of morphological simplifications in FE modeling and experiments on their mechanical behavior.

Thus, this study aims to bridge the gap between the 3D morphological complexity of sutures and their impact on craniofacial mechanical properties. The experiments aim to apply loading to a suture and use imaging techniques to retrieve morphological data. Using both pieces of information from the suture, a statistical model can be used to find

correlations and predict the suture's morphological properties which are most important for predicting its bulk mechanical properties.

3.2 Methods

3.2.1   Swine Suture Dissection and Measurements

Nine maxillae containing the internasal suture were collected from swine obtained from the Surgical Medical Research Institute (SMRI) of the University of Alberta through a secondary use ethics exemption (reference number: ETR24) from the University of Alberta Research Ethics Office. The maxillae were collected immediately after euthanizing, using an oscillating electric surgical bone saw at the approximate location of the nasofrontal suture. The maxillae were then frozen at -24°C until the experiments for this study were carried out.

To prepare samples for the experiment, the previously frozen maxillae were left in a 0 °C refrigerated room for 24 hours. At the beginning of the dissection, the outer surface of the nasal bone in the maxilla was skinned and the bare bone with the internasal suture was exposed (Figure 6). The skinned maxillae always revealed that the nasofrontal suture was located near the eyes of the swine, which is the posterior region of the maxilla (Figure 6). To ensure consistency of locations of posterior and anterior regions, the samples were dissected from the same anatomical region and controlled to the width of 5mm (Figure 6). The region of the internasal suture that was closest to the nasofrontal suture (Figure 2) was defined as the posterior region. The internasal suture sample closest to the nostrils was considered the most anterior region. The internasal suture and the surrounding bone from the most posterior to the anterior region were then cut into approximately 5 mm sections using an electric oscillating saw as shown in Figure 6. At the end of the dissection, all samples included a part of the internasal suture and the surrounding bone. The samples were tested immediately after dissection.
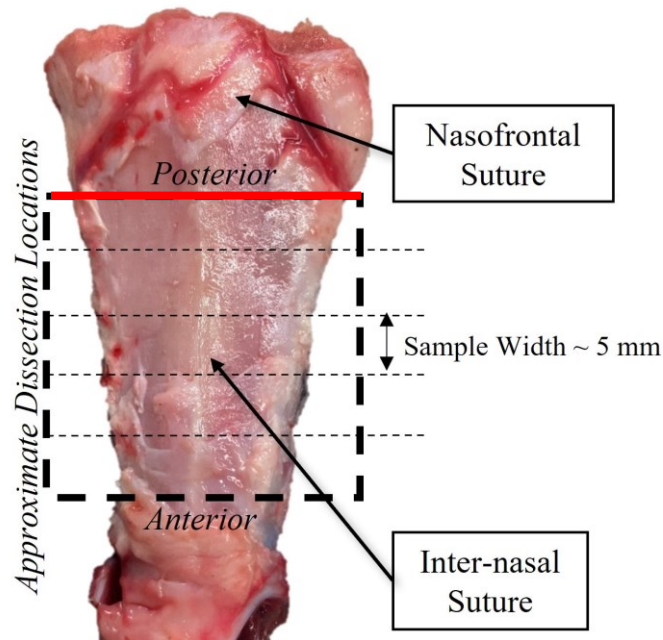
Figure 6: Maxilla dissection regions showing nasofrontal suture location, anterior and posterior regions, and dissection locations in dashed lines

After dissection, the sample thickness (Figure 7), from the outer to the inner surface of the nasal bone, at the location of the internasal suture, was measured using a digital caliper. The sample width (Figure 7), which is controlled to be approximately 5mm, was also measured using the digital caliper. The origin (red line in Figure 6) was taken as the position from which most posterior sample was dissected, while the most anterior sample was closest to the nostril (Figure 6). To measure the position of each sample in the maxilla, the distance from the origin (red line Figure 6) to the midpoint of the sample was calculated. The distance to midpoint of a sample was calculated by dividing the sample width by two and calculating the distance from the origin of the maxilla. Additionally, one of the swine maxillae had six samples, while the rest had between four and five samples. The goal was to compare samples from different maxillae based on their relative position, starting from the posterior region closer to the nasofrontal suture. To ensure consistency, a maximum of five samples from each maxilla was used. All sample measurements including sample width, thickness and position are mentioned in Appendix A.

22
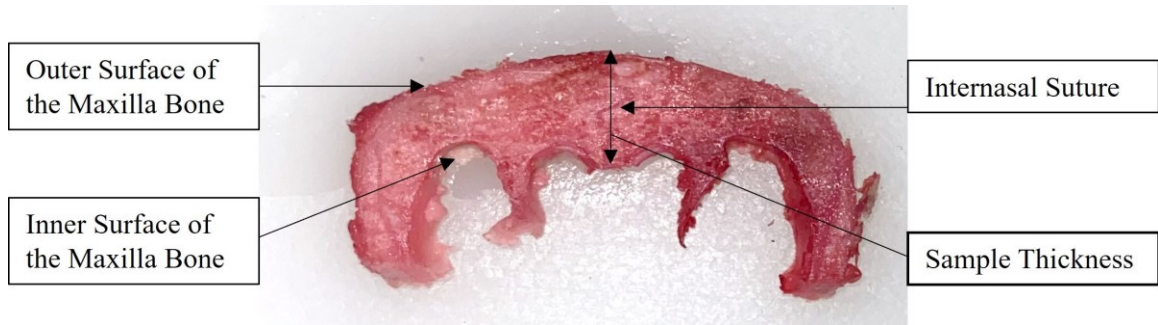
Figure 7: Coronal view of a sample with internasal suture and dimensions

3.2.2 Mechanical Experiment

An Instron Electroplus E3000 material testing machine (Instron, Norwood, MA) with 50 N load cell and 1kN manual wedge grips attached was used to apply a uniaxial tensile load to the sample. The measurements of interest from the Instron setup were the output force and crosshead displacement measurements. When mounting the sample on manual wedge grips, it must be aligned with the internasal suture running in the middle of the region outside the grips (Figure 8). Additionally, the grips should be tightened securely to prevent slippage.
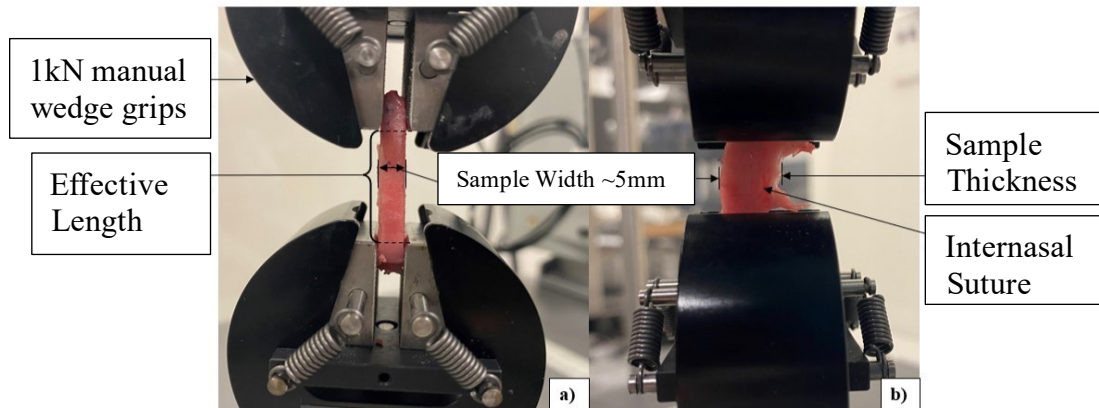
Figure 8: Sample mounted on manual wedge grip in Instron Electroplus E3000 material testing machine for mechanical testing

The mechanical experiment consisted of three stages: preload, preconditioning, and loading. The actuator was displaced at a 0.2 mm/min rate throughout the experiment to

achieve the desired load or displacement. This displacement rate was chosen so that the suture was displaced at a quasi-static rate [23].

A preload was important in the experiment to ensure that all the samples started with the same initial loading condition. When the sample was mounted to the miniature grips, there could be small compressive or tensile loads that resulted from the tightening of the grips. Therefore, it was necessary to apply a preload of 0.5 N at the start of experiments [23,58].

The samples were then subjected to preconditioning to ensure that all sutures started at a similar state. Preconditioning was displacement-controlled cyclic loading from 0.5N to 1N [59,60]. The 20 preconditioning cycles were selected for the preconditioning step after it was observed that the cycles achieved a repeatable state. Preconditioning changes the internal structure including collagen fibers, water, and other components of the suture. With repeated cycling a steady state with predictable behavior will be formed [61]. During preconditioning, the peak displacement of preconditioning cycles as a percentage of change from the previous cycle was observed to be less than 5% for all samples after 20 cycles. The preconditioning step has been used to ensure that samples start the next stage at a repeatable/ predictable state and all sutures have experienced the same loading conditions.

In the third stage of the experiment, tensile loading was applied to the bone-suture-bone sample at a rate of 0.2 mm/min. This step is displacement controlled where a maximum displacement achieved was 0.3 mm and a maximum load was set at 20 N. Similar bone-suture-bone tensile tests on pigs had higher peak stress and strain values and failure regions than the selected values [23]. The goal of the present study was to observe the region before failure for the dissected internasal samples. The linear region of load vs data obtained from this experiment can be used to obtain the uniaxial stiffness of the sample as described in using linear regression of the truncated region.

3.2.3   µCT X-ray Imaging and Image Processing

The samples were scanned at 9 μm nominal resolutions with 90 kV source voltage, 278 μA source amperage, 0.7° rotational steps, and 1 mm aluminium filter using a SkyScan 1176 μCT (Bruker-SkyScan, Kontich, Belgium). The raw datasets were reconstructed using NRecon Version 1.6.3.3 (Bruker-SkyScan, Kontich, Belgium) where they were

converted into 2D cross-sectional slices in the coronal view through the sample. The reconstructed datasets were imported to DataViewer Version 1.4.3.2 (Bruker-SkyScan, Kontich, Belgium) where they were reoriented in 3D and cropped so that the internasal suture was orthogonal to the image planes as shown in Figure 9. The sample thickness was approximately 5 mm for each sample. It was observed that it was difficult to distinguish bone from sutures at either side of sample, at dissection locations, since those regions were affected by the bone dust due to the sample dissection process. Thus, some of the image slices were removed from the dissection locations by visual inspection. From the remaining μCT image data set, 11 images were selected though the sample thickness of 5 mm, at 10% increments.

The selected 11 μCT images were processed using a method developed previously by Remesz et al[16] with MATLAB R2020A (MathWorks, Natick, USA). MATLAB scripts are in Appendix C. A single slice from a sample will be used to show the image analysis process (Figure 9a). Figure 9b shows the image slice that has been cropped to only focus on the area of the bone where the internasal suture exists. Figure 9c is the resulting image after the image has undergone thresholding, and binarizing. Thresholding was used to determine the region of the image that will be converted to black or white during binarizing. Binarizing process turn the suture and other porous regions in the bone to white color and bone to black color. Finally, in Figure 9d, only the suture area was isolated using the segmentation process of removing surrounding bone and identifying the suture's top and bottom extremities.
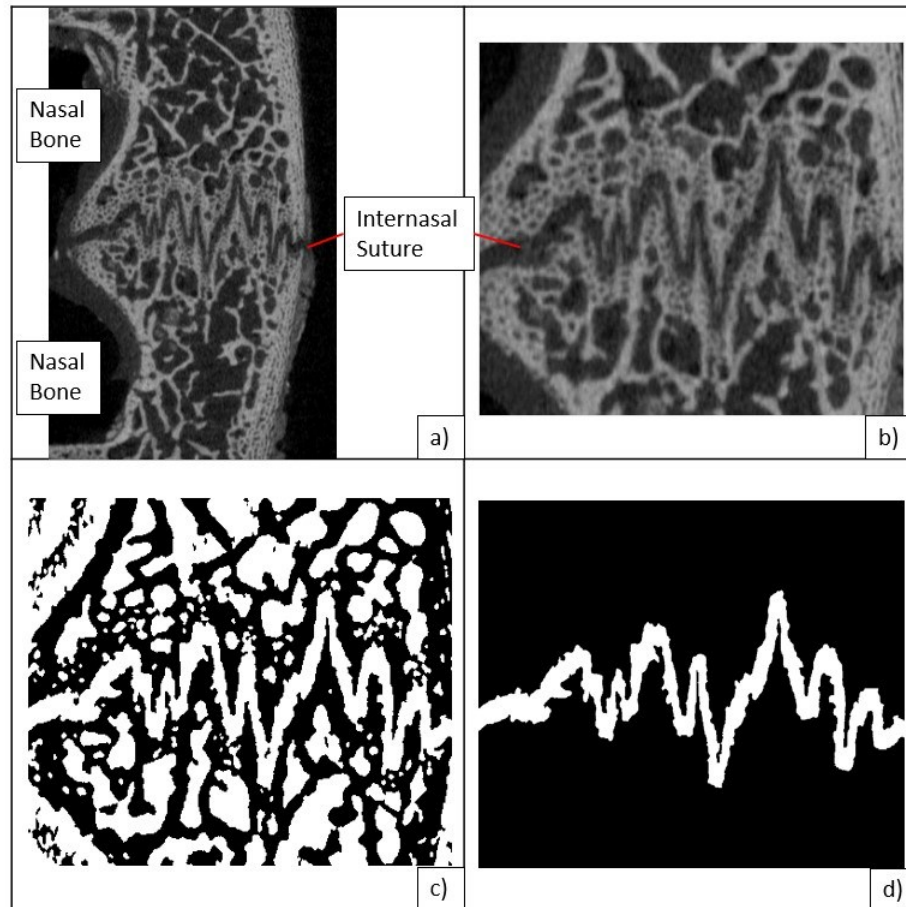
Figure 9: Processing of a µCT image slice using MATLAB Code a) µCT image slice from the coronal view b) cropped image c) binarized image d) isolated suture area in white and surrounding bone in black

MATLAB R2020A code from Remesz et al [16] study was used to extract morphological information from the segmented images. Firstly, the segmented suture from the previous step, was used to trace suture boundary to identify the top and bottom edges of the suture (Figure 11). Some modifications were used to make the analysis more suitable for the internasal suture (MATLAB scripts in Appendix C). The MATLAB code used by Remesz et al [16] could not identify regions with high curvature, which was traced in cyan colored lines in Figure 11. The code used by Remesz et al generated the top and bottom edge curves of the suture (Figure 11) of the suture. It then started on the left side of the suture and determined the suture width by calculating the closest distance between the top and bottom curves. The code progressed along the suture by determining the center point of suture width line (pink lines in Figure 11) and finding the next center point by advancing three

pixels normally to the suture width line. In the modified code the center points of the suture were predetermined using a skeletonization process. The skeletonization process uses the `bwskel` function in MATLAB to reduce the binary segmented suture image to a 1-pixel wide line, by reducing pixels from the outer boundaries while keeping the essential structure of the suture preserved (Figure 10). This process uses the Medial Transform Axis (MAT)[62], which is a mathematical model that determines the distance of image pixels to the background to remove pixels from the outer most edges of the image. As MAT process is repeated, the pixels from the image outline will be removed to until only the center line of the image remains. In this study, the image will be the segmented suture. The suture skeleton is shown in Figure 10. The `bwskel` function in MATLAB was used with a minimum branch length of 100 to eliminate branches generated in the skeletonization process to obtain the center line (red line in Figure 11).
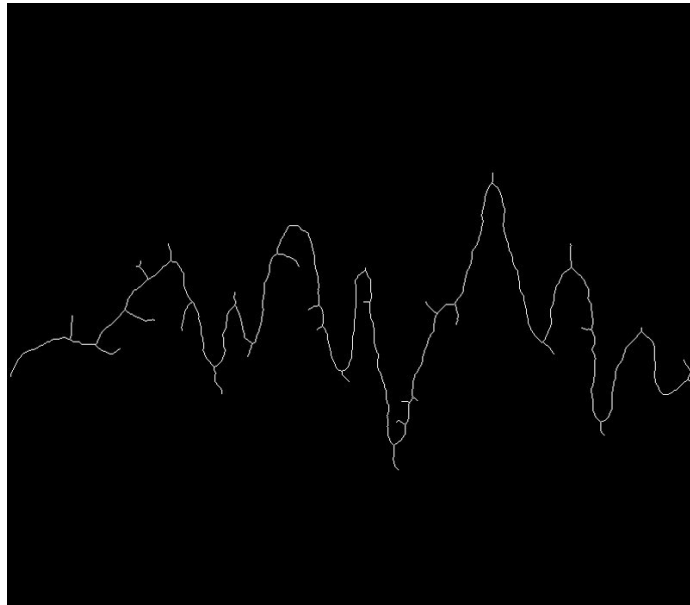
Figure 10: Skeletonized image of the segmented suture with the branches that encompass the suture area

From each pixel of the center line, a range of 180° with 1° angular steps was scanned to find the closest distance between the top and bottom curves. The closest distance was the suture width at the center point (shown in pink lines Figure 11). Additionally, if the angular space between two pink lines from two center points next to each other was greater than

10 degrees, the space between these two lines were divided into equal sections with 5˚ angular span between each section. Then, vectors are created between these points (shown in cyan lines Figure 11) and used to find the suture width in the space by finding distance between intersection points of the top and bottom curves.
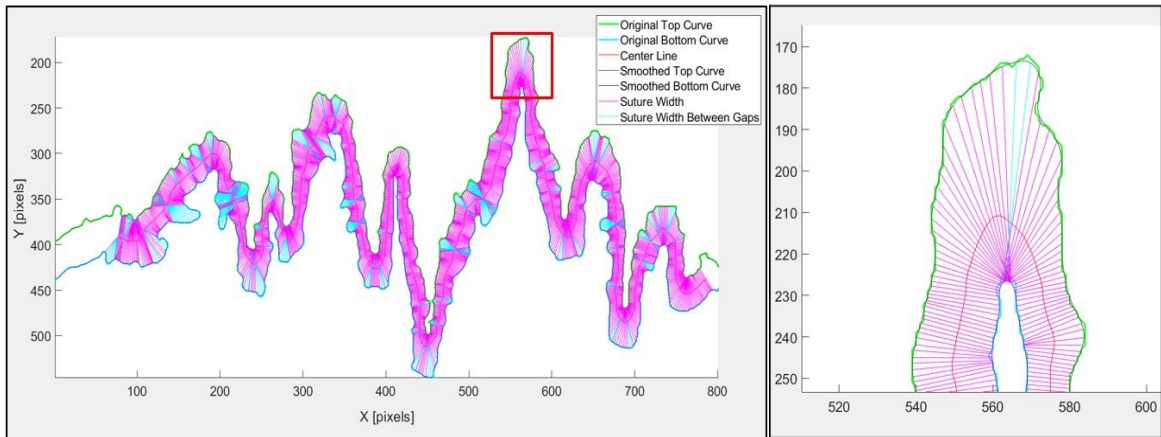
Figure 11: MATLAB code output of morphological analysis for a μCT image slice from a sample

The suture width found at each pixel within the single image slice was averaged to find the suture width of the segmented suture slice. This way, for each sample, 11 measurements of suture width are found through the thickness of the sample. Then, for each sample the minimum, maximum, and average values for suture width from the 11 measurements were found.

To find the suture LII, the length along the skeletonized center line was divided by the linear distance between the two edges of the suture center line. LII was also measured for all 11 images for each sample and the average, minimum, and maximum suture LII for each sample were found. All morphological data are mentioned in Appendix D.

3.2.4   Statistical Model

The statistical model was developed using data from 42 samples taken from nine different swine maxillae. Stiffness data obtained from the mechanical experiment was used to determine if there was a significant difference in variability between the data obtained from different swine maxillae. To use one-way ANOVA method to compare maxillae, the

28

stiffness data from each maxilla need to be normally distributed [63]. Kruskal-Wallis test was used instead of one-way ANOVA to compare groups because each swine maxilla only had 4-5 samples, and it was impossible to determine if data from individual groups were normally distributed [63].

Hypothesis test for Kruskal-Wallis test, where null hypothesis is H_0 and alternative hypothesis is H_1:

H_0: There was no variability between uniaxial stiffness data from different maxillae

H_1: There was variability between uniaxial stiffness data from different maxillae

If Kruskal-Wallis test found that there was significance variability between stiffness data, the data should be grouped according to the corresponding maxilla. If there was no significant variability, 42 samples can be analyzed as one group without the consideration of their maxilla.

All morphological, physical, positional, and mechanical variables were considered for the statistical analysis. The study collected morphological data such as suture width and LII, physical measurements such as sample thickness, positional measurements such as the sample position in the maxilla (measured from posterior to anterior region), and mechanical variables taken from the tensile test data. The mean, minimum, and maximum suture width and LII values were obtained from 3D μCT data analysis for each sample. During the dissection, the sample thickness was measured using a digital caliper (Figure 7). The sample width is controlled to be approximately 5 mm for all samples (Figure 6); thus, it was not included for statistical analysis. The sample position in the maxilla was considered as a variable that can be used for comparison between maxillae, since the samples were dissected from the same anatomical regions (from the posterior to anterior region). Finally, uniaxial stiffness measurements from the load vs. displacement data for each sample were taken as the mechanical property.

Multiple regression was used to study the correlations of internasal suture morphology and mechanical response to tensile loading. The multiple regression model included mechanical, morphological, physical, and positional data obtained from 42 samples collected from 9 swine maxillae. The number of available samples is a key determinant of

the statistical power of a regression model [63,64]. An acceptable statistical power ($1-\beta$) and a significance level (α) were needed for a multiple regression model to avoid type I and II errors. G*Power software (version [3.1.9.6]; Franz Faul, University Kiel, Germany) can be used to carry out a power analysis for the multiple regression model [63,64]. It uses calculation methods used by Cohen et al [65] which uses sample size, number of independent variables, and significance level (α) to determine the statistical power ($1-\beta$) of the model using ANOVA[65]. A significance level (α) of 0.05 used in this thesis since it was widely used in literature and avoids type I error[63,64].

Probabilities of type I and II errors, where H_0 is the null hypothesis of multiple regression model and H_1 is the alternative hypothesis:

$\alpha = P(\text{type I error}) = P(\text{reject } H_0 | H_0 \text{ is true})$

$1 - \beta = P(\text{type II error}) = P(\text{fail to reject } H_0 | H_0 \text{ is false})$

Multiple regression was performed with JASP software (version [0.17.2.1]; JASP Team, 2023)[61] with the independent variable as the uniaxial stiffness from the load vs. displacement data, and dependent variables as the morphological, physical, positional, and mechanical variables described earlier. After performing Kruskal-Wallis test as previously mentioned, it will be determined if data will be grouped in the multiple regression model according to their swine maxilla.

The equation for multiple regression is[63]:

$$Y = C_0 + C_1 x_1 + C_2 x_2 + C_3 x_3 + C_4 x_4 + C_i x_i \ldots \qquad \text{Equation 2}$$

for each independent variable added $i = 1, 2, \ldots, n$

Where Y is the dependent variable (stiffness), $x_1, x_2, x_3, x_4, \ldots$ are the independent variables (suture width, LII, sample thickness, sample position, swine maxilla the sample was dissected), and $C_1, C_2, C_3, C_4, \ldots$ are regression coefficients that describe the relative effect of each independent variable on predicting the dependent variable.

Hypothesis test for multiple regression model:

$H_0: C_i = 0$ (Independent variable had no effect)

$H_1: C_i \neq 0$ (Independent variable had a statistically significant effect)

The rejection of null hypothesis ($\alpha < 0.05$) results in the independent variable related to the regression coefficient under consideration, having a significant impact on the independent variable.

The multiple regression model also needs to be tested to see if all assumptions were met[66]. When assumptions are violated, the performance of the multiple regression model will be negatively impacted[63]. Assumptions of independence of observations, linearity, normality, and homoscedasticity needed to be met[61,63]. Additionally, there should be no multicollinearity between any of the independent variables and no outliers [61,63]. These assumptions were also tested using JASP software (version [0.17.2.1]; JASP Team, 2023)[61]. Durbin-Watson test checked for correlation between residuals, and it should ideally be 1-3 in value[68]. If there is no correlation between residuals, it can be concluded that the observations (predicted values) from the regression model are independent [61]. Linearity ensures that there is a linear relationship between dependent and independent variables [61]. Homoscedasticity ensures that there is homogeneity of variance for predicted (difference between predicted and actual data of the independent variable) values of the independent variable [61]. If there are no obvious patterns (randomly distributed) in residuals vs predicted values plot from the multiple regression model, these assumptions are met [61]. Normality assumption can be verified using a Q-Q plot (standardized residuals against the theoretical quantiles) [61] and the data points should follow diagonal line though the origin[61]. This assumption ensures that residuals are normally distributed, and ANOVA can be used. Multicollinearity between independent values can be checked using tolerance and VIF (variance of inflation factor) [61]. A VIF value of less than 5 and a tolerance greater than 0.2 indicated acceptable collinearity statistics. Ideally the VIF value should be 1 to have no multicollinearity [68]. Outliers are identified if the standardized residuals (residual divided by the standard deviation of residuals of independent variable) are greater that ± 3 standard deviations [61]. When all assumptions of multiple regression are met, the results of the statistical model can be used to derive correlations between stiffness and morphological, positional, and physical properties of the internasal suture samples.

3.3 Results

3.3.1 Mechanical Test Analysis

The mechanical test was designed to apply a pure tensile load to the swine bone-suture-bone sample. Preconditioning was done at a load range of 0.5-1N after preloading the sample to 0.5 N. All samples underwent 20 cycles of loading within this range to ensure predictable and repeatable starting conditions before tensile testing[61,67]. An example of the preconditioning cycles for a sample is shown in Figure 12. Here, data were displayed using MATLAB R2020A `smooth` function, which uses moving average method (finding average of five consequent data points at each data point to identify the overall trends of data) to remove noise and visualize the cycles. Figure 12 shows an increase in displacement with each preconditioning cycle, converging of the cycles, and a decrease of the hysteresis loop area, which is consistent with observations in literature [61,67].
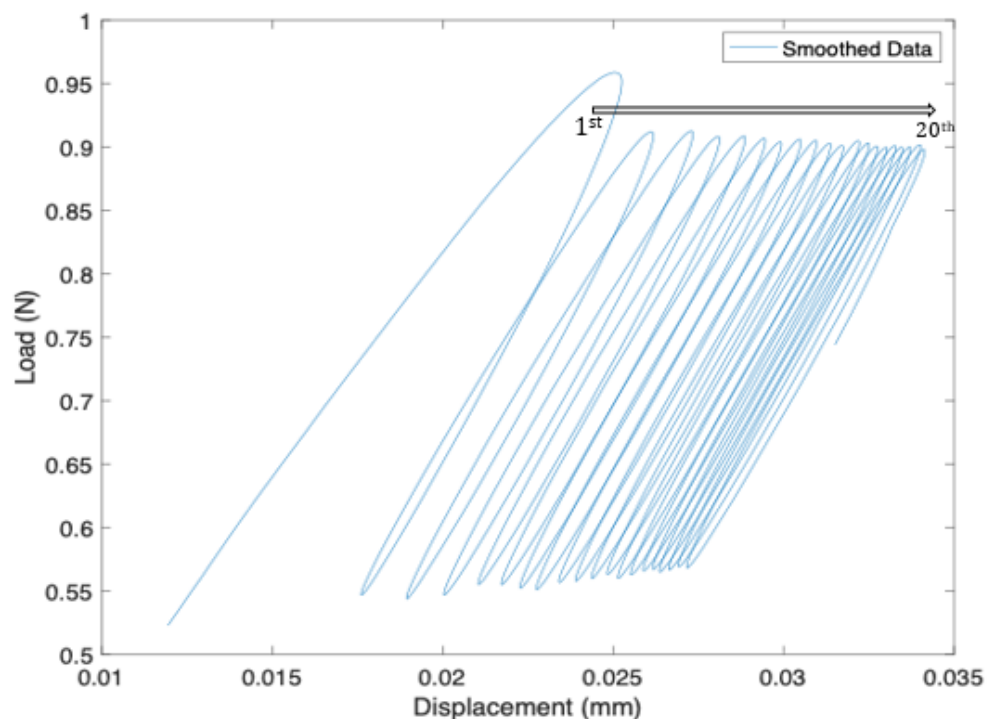
Figure 12: Smoothed load vs displacement data during preconditioning for one maxilla sample (preconditioning consisted of cyclic loading between 0.5-1 N with 20 cycles)

To numerically assess if preconditioning samples were converging, the change in displacement at the maximum load (DM) of each cycle from its previous cycle was calculated as a percentage, for all 20 preconditioning cycles (Equation 3). This was calculated for all 42 bone-suture-bone samples that were mechanically tested across the 9 maxillae and represented in Figure 13. Each data point on the graph represents a sample, with the percentage change of displacement at maximum load on the y-axis and the corresponding preconditioning cycle on the x-axis. It shows that after 20 preconditioning cycles, all 42 samples reached convergence as the percentage change in displacement reached at highest load was less than 5%.

$$\text{Pecentage change } (\%) = \frac{\left(\text{DM } n^{\text{th}} \text{ Cycle}\right) - \left(\text{DM } n - 1^{\text{th}} \text{ cycle}\right)}{\text{DM } n^{\text{th}} \text{ cycle}} \qquad \text{Equation 3}$$
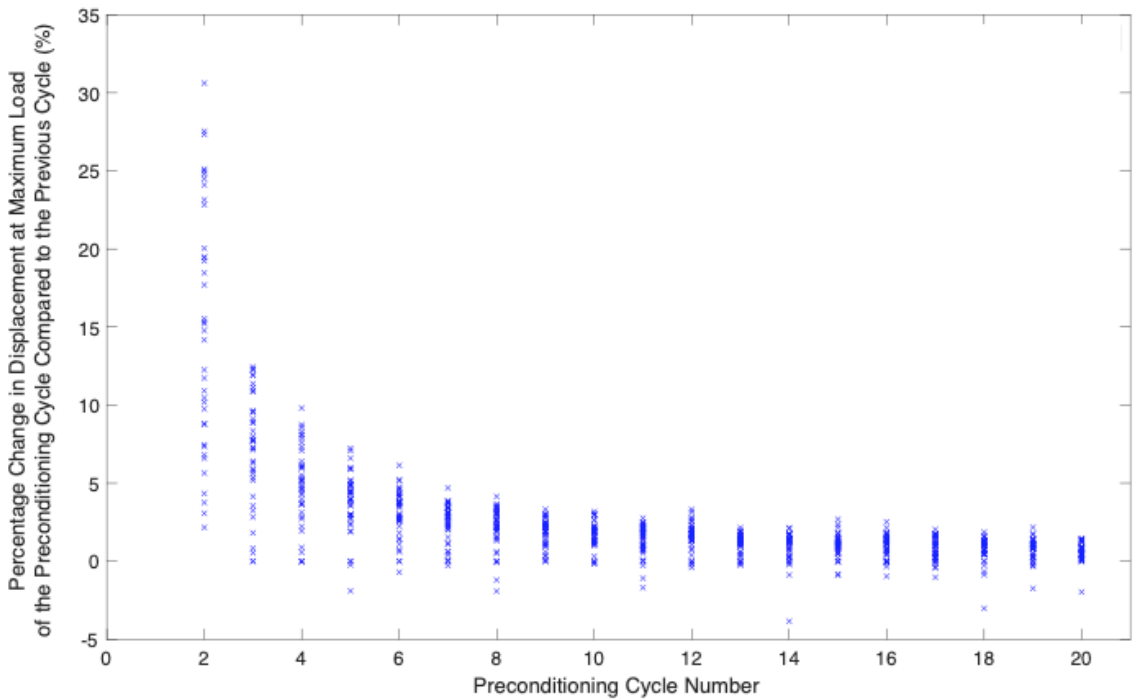
Figure 13: Data shown for percentage change data (Equation 3) of 20 preconditioning cycles (x-axis) of all 42 bone-suture-bone samples (There are 42 data points for each cycle number in x-axis)

The early stage of the tensile loading had a non-linear region (Load vs displacement data for one swine maxilla is shown in Figure 14, Data for all maxillae is in the Appendix

B.1). It was deduced that this region was not a by-product of the preconditioning stage because the same behavior was observed during pilot tensile tests when the sutures were not subjected to preconditioning. The initial 10% of load vs. displacement data were removed to obtain material properties of the linear region after the initial nonlinear region. This practice was commonly used in literature to account for the rearrangement of collagen fibers[22,23,61]. The initial toe region is removed, and only the linear region is considered to calculate the stiffness of biological materials during material testing[22,23,61].
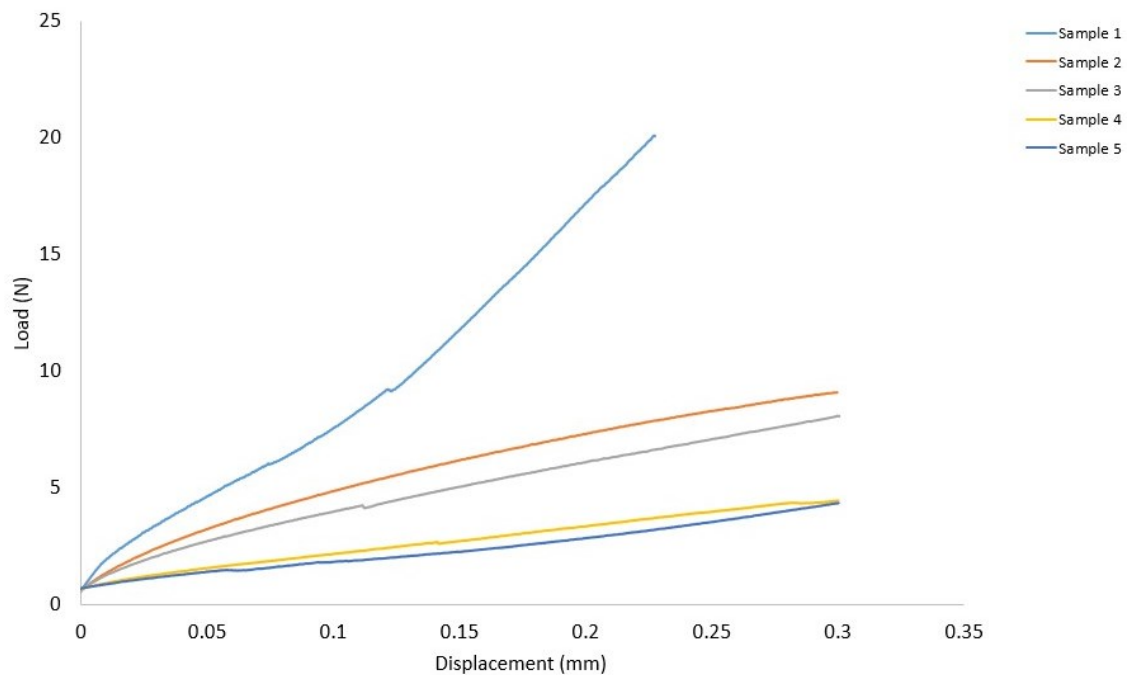
Figure 14: Load vs. displacement data for a representative swine maxilla

Figure 15 shows the truncated load vs. displacement data (initial 10% removed) for samples of a representative maxilla (truncated load vs displacement data for all samples and their linear regression fits are in Appendix B.2). These truncated data were fit to a linear regression model and the gradient of the linear model represents the uniaxial stiffness, which will be used as the independent variable for multiple regression model. The R^2 values from the linear regression fits in Figure 15 were above 0.9 in every sample showing that the relationship between truncated load vs. displacement data was linear with minimal variability. R^2 value represents the proportion of variance of the dependent variable and the goodness of fit in the regression model.

34

Tension test results for samples typically taken from the posterior regions of maxillae, showed that the suture went from a linear to a nonlinear region at higher loads, when the load vs displacement measurement began a nonlinear upward trend (Figure 14). In general, posterior samples nearer to the nasofrontal suture reached a higher load compared to anterior samples, often exceeding 10N. This indicates that these sutures have greater stiffness resulting in higher loads achieved with the same amount of displacement compared to anterior samples. In Figure 14, sample 1 is the most posterior sample, and sample 5 is the most anterior. Sample 1 from all swine maxillae had a uniaxial stiffness in the rage of 23.9-99.7 N/mm while sample 5 had 7.74 – 29.8 N/mm (Appendix B.2).

Figure 16 shows the summarized uniaxial stiffness values (gradient values of load vs. displacement data) separate by maxilla. The gradient of load vs. displacement data was a measurement of the uniaxial stiffness of a sample under tensile loading since the displacement was only measured in one direction by Instron Electroplus E3000 machine.
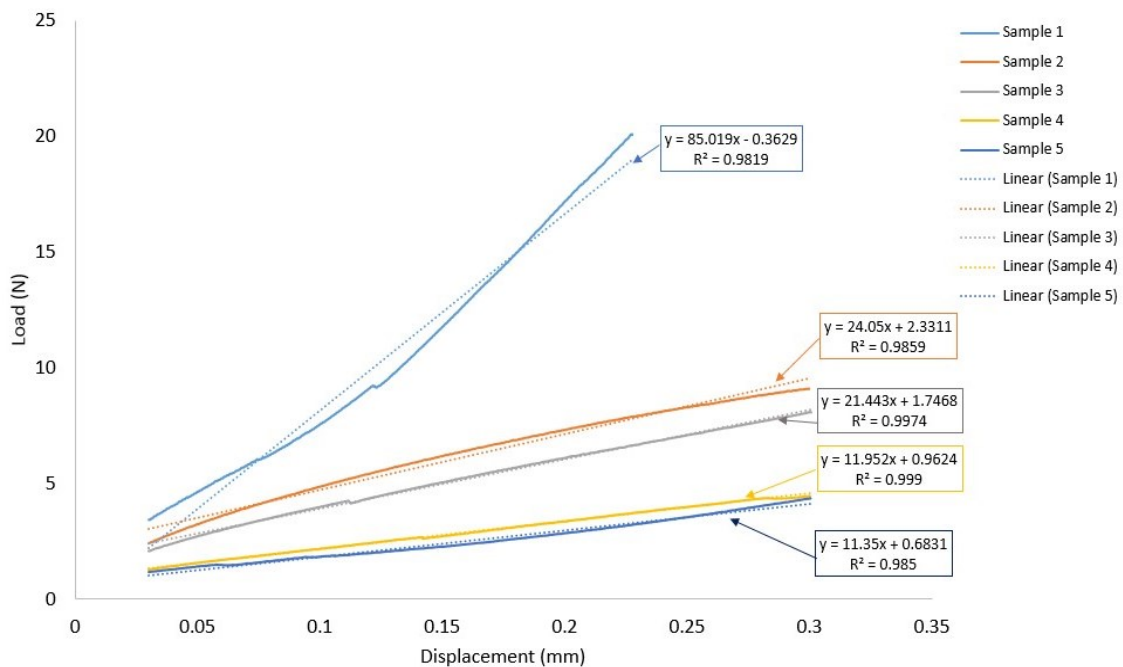
Figure 15: Load vs. displacement data with initial 10% of data removed for a representative swine maxilla, the slope of the data obtained through linear regression fit represents the uniaxial stiffness and R2 value
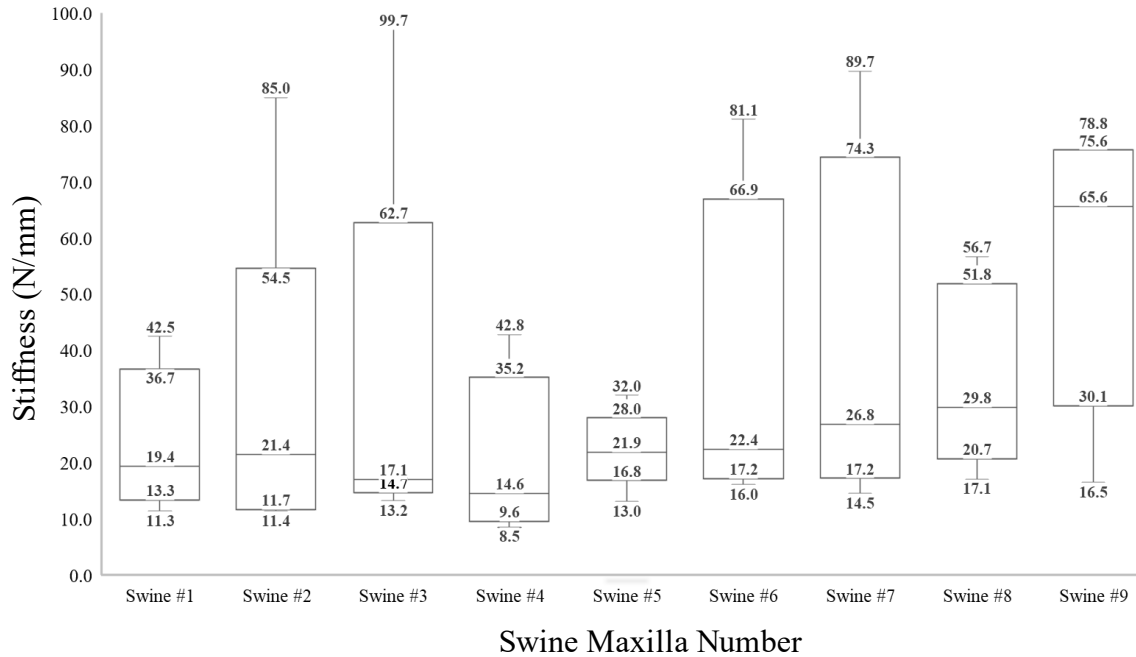
Figure 16: Box plots of gradient of load vs displacement data of tensile tests against swine maxilla

3.3.2 Image Analysis

The results of image analysis show that the mean, minimum, and maximum values of suture width for all samples are highly correlated with each other (Table 1). This was also true for suture LII mean, minimum, and maximum values (Table 1). Pearson correlation coefficient (r) measures the linear correlation between two sets of data. All combinations between minimum, maximum, and average values of suture width and LII data for 42 samples, had a Peason's r greater than 0.95 showing high positive correlation. As a result, it was evident that the morphology change through the thickness of the suture was not significant. If all minimum, maximum, and mean values of suture width and LII were used as independent variables in the multiple regression model, there will be multicollinearity between these variables, which would be in violation of the multicollinearity assumption in multiple regression[66]. For this reason, only the mean values of suture width and LII will be included in the multiple regression model.

36

Table 1: Correlations between minimum, maximum, and mean values of suture width and LII

	Pearson's r
Suture Width	
Minimum - Maximum	0.952
Minimum - Mean	0.989
Maximum - Mean	0.977
Suture LII	
Minimum - Maximum	0.957
Minimum - Mean	0.989
Maximum - Mean	0.985

3.3.3   Statistical Analysis

Kruskal-Wallis test was used to determine if there was significant variability between uniaxial stiffness data from different swine maxillae. Kruskal-Wallis test was analysed using JASP software version [0.17.2.1]; JASP Team, 2023[68] with a 95% confidence level, 9 maxillae groups, each with 4-5 samples. The statistical significance (p-value) was 0.452, which was P value greater than 0.05, and there was not enough evidence to reject the null hypothesis that there is no variability between stiffness results from different maxillae (Table 2). Thus, it was concluded that stiffness data from all 42 samples were independent of their swine maxilla. Since data from swine maxillae were independent, it was possible to compare them with each other, and the swine maxilla that the sample belongs to was not a factor that is needed in the multiple regression model.

Table 2: Kruskal-Wallis test, JASP software (version [0.17.2.1]; JASP Team, 2023

Factor	Statistic	df	p
Swine Maxilla #	7.810	8	0.452

G*Power software (version [3.1.9.6]; Franz Faul, University Kiel, Germany) was used to carry out a power analysis for the multiple regression model[63,64]. G*Power software was used to obtain the resultant power (1-β) of the model with a significance level (α) of 0.05, 4 independent variables, and 42 number of samples. It was found that the multiple regression model had a resultant power of 0.99. It was evident that this model would predict the most significant independent variables while avoiding type I and II errors.

Multiple regression model was used to predict the uniaxial stiffness value of swine internasal samples with the use of independent variables, mean suture width, mean suture LII, sample thickness, and sample position in the maxilla. Firstly, the data set was to be tested to see if all assumptions required for multiple regression were met[68]. Assumptions of linearity, normality, multicollinearity, and homoscedasticity were met as discussed below, and analyzed using JASP software version [0.17.2.1]; JASP Team, 2023[63,66,68]. The data had no outliers in the standardized residuals. The Q-Q plot (Figure 17) shows standardized residuals against the theoretical quantiles. The fit along the diagonal lines suggests that the assumptions for normality have been met[68].
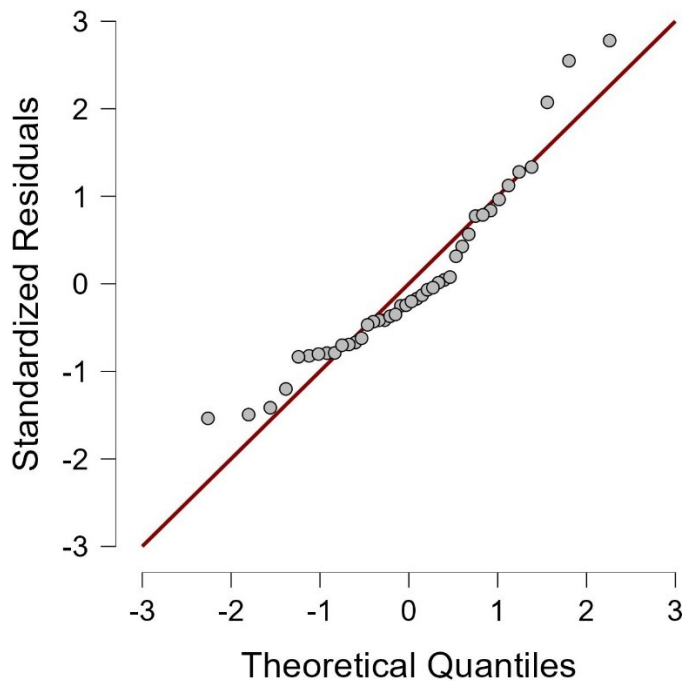
Figure 17: Q-Q plot of the multiple regression model with standardized residuals vs theoretical quantiles

Figure 18 shows the residuals vs. predicted data for the multiple regression model. The residuals are almost evenly dispersed above and below the zero line, and there are no obvious patters in the distribution, suggesting that homoscedasticity and linearity assumptions have been met [68].
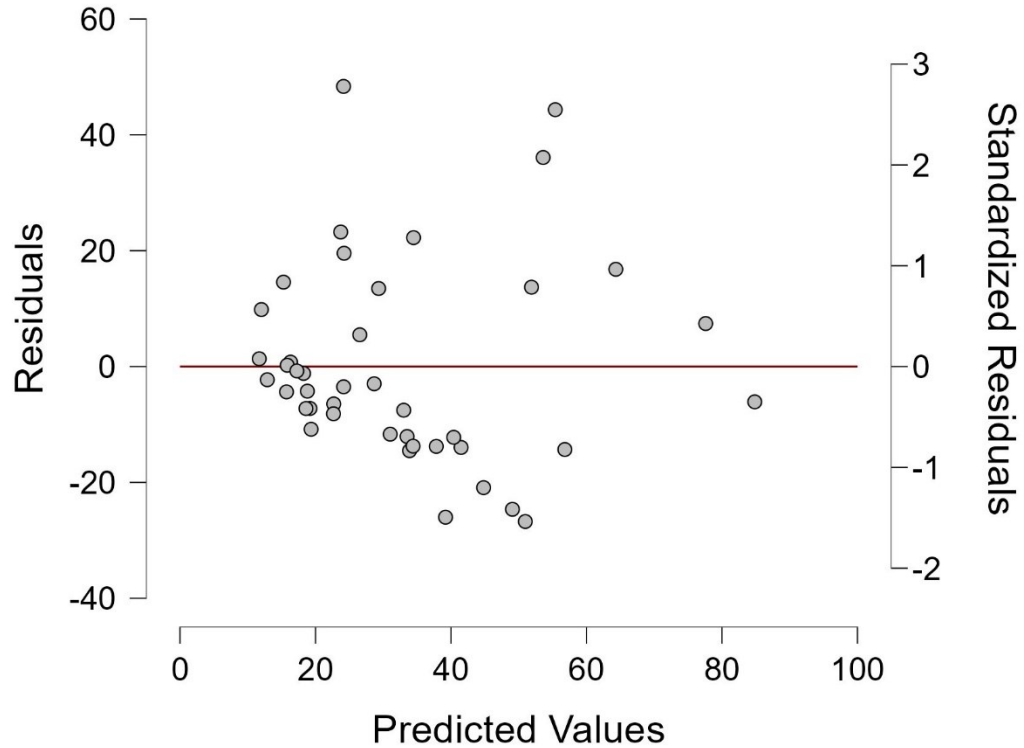
Figure 18: Residuals vs. predicted values for independent variable: gradient values of truncated load vs. displacement data

The residuals in multiple regression model had a Durbin-Watson statistic of 2.015, showing no correlations between residuals[68]. Additionally, the tolerance and VIF (variance of inflation factor) checked for multicollinearity. VIF values for all independent variables were less than 5 and the tolerance was greater than 0.2, which indicated acceptable collinearity statistics (Table 3).

Table 3: Tolerance and VIF (Variance Inflation Factor) to test for collinearity in independent variables

	Tolerance	VIF
Thickness	0.355	2.817
Mean suture width	0.690	1.450
Mean LII	0.527	1.898
Position	0.329	3.043

The results of the multiple regression model showed that the independent variables can predict the gradient with statistical significance; $F_{(4, 37)} = 9.513$, p-value less than 0.001. The R^2 and adjusted R^2 values were used to explain the proportion of variance explained by the four independent variables. The R^2 value for the model was 0.507 and the adjusted R^2 was 0.454. The adjusted R^2 showed that the model can predict 45.4% of the resulting variation of the multiple regression model.

In addition, as shown in Table 4, two out of the four independent variables were statistically significant in the model. The mean suture width negatively predicted the gradient (p value = 0.03), such that an increase in suture width decreased the gradient. The sample thickness positively predicted the gradient (p value 0.005), while the mean LII and sample position were not significant (had p values greater than 0.05). The standardized coefficients in Table 4 showed the relative magnitude of the effect of independent variable on the dependent variable prediction. It was clear that thickness and suture width had the highest effect. The unstandardized coefficients are the regression coefficients C_i of the multiple regression model. The p value for null hypothesis H_0 in Table 4 is less that 0.001, showing that there is low probability of it being true. This allows for the rejection of null hypothesis. The implications of statistical model findings are explained in Section 3.4.

Table 4: Multiple regression independent variable standardized and unstandardized coefficients, p values

Model		Unstandardized	Standardized	t	p
H_0	(Intercept)	32.995		8.627	<.001
H_1	(Intercept)	32.013		0.691	0.494
	Mean SW	-28.070	-0.313	-2.253	0.030
	Mean LII	-4.878	-0.107	-0.673	0.505
	Thickness	13.189	0.583	3.009	0.005
	Position	-0.509	-0.141	-0.700	0.488

3.4   Discussion

In the beginning of the load vs displacement measurement data, a nonlinear region was observed. This region could be a result of the internal material structure of the internasal suture. In a previous study, it was reported that when the maximum load and displacement in the tensile loading stage of human tendon surpassed the values reached in the preconditioning stage, the collagen fibers and material components were further rearranged and displaced[61]. This will create regions resulting from the internal structure of the suture material components. In another previous study that applied tensile loading to failure for the swine nasofrontal suture, the maximum stiffness of the mechanical data was observed during low loads[23]. This indicated that the collagen fibers in the nasofrontal suture were arranged to resist tensile loading immediately with loading[23].

Typically, samples with higher stiffness from posterior region of the swine maxilla went to a nonlinear region at higher loads since they showed an upward trend in the load vs displacement data (Figure 14: Load vs. displacement data for a representative swine

maxilla). The peak load values reached here were less than the load ranges seen on tensile tests at low rates on swine cranial suture samples of nasofrontal sutures in literature, which was 50-60 N[23]. Nonlinearity of data were expected since cranial sutures are made of a complex material structure that effects their mechanical properties[61]. In a previous study that applied displacement to ex vivo samples of rat coronal and sagittal sutures, the load vs displacement curves had an initial toe region followed by a linear region before failure [22].

From the imaging data, the 3D morphology of the internasal suture can be observed. The suture will not experience a purely tensile load at it's every location due to the complex 3D morphology[23]. As reported in previous literature, shear and bending forces are expected to be generated in the suture due to its morphology[23]. Additionally, the curved shape of the maxilla did not follow the ideal dog bone shape that was required for an ideal tensile test[69]. This also contributed to the distribution of tensile stress throughout the sample. However, the forces experienced in the swine maxilla in reality will not also be purely tensile due to its complex material composition and morphology[23].

Imaging data revealed the composite structure of the nasal bone with an inner porous layer and a denser outer layer, as shown in Figure 19. In this thesis, it was assumed that the displacement applied during the experiment was undergone by the suture instead of the bone. The affect of the nasal bone to the mechanical response of the bone-suture-bone sample was not considered since it was reported in literature that the bone was significantly stiffer and had higher elastic modulus compared to the suture[1,8]. For example, it has been reported in a study that applied tensile and compressive tests to bone-suture-bone samples of the swine nasofrontal suture, that the suture experienced a much higher deformation than the bone[23]. Additionally, it was assumed in this thesis that the load measured by the Instron Electroplus E3000 material testing machine (Instron, Norwood, MA) is the load experienced at the internasal suture. In previous studies that applied loading to bone-suture-bone samples, the load vs displacement response was used to find the mechanical properties of suture[22,23]. For an example a study that applied tensile tests to bone suture-bone samples of coronal, posterior frontal, and sagittal sutures of Wistar rats, the linear portion of load vs displacement data was used to find suture stiffness[22]. In future

work, a FE model can be used to find the effect of bone structure to the stress distribution, by modelling it as a composite structure.
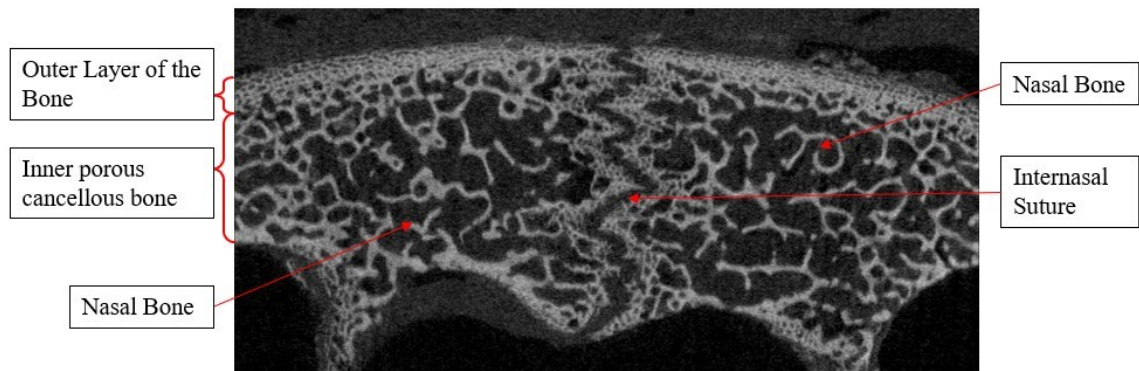
Figure 19: Cross Section of a Sample Showing the Structure of Nasal Bone

From the statistical analysis using multiple regression model, it can be concluded that in this test that applied tensile loading to internasal suture, only the average suture width and thickness of the sample influenced the uniaxial stiffness with statistical significance. A higher sample thickness would result in a larger cross-sectional area (sample width × sample thickness) since the sample width was controlled to approximately 5 mm during dissection. With a larger cross-section of the sample, there will generally be more suture material with sample material and mechanical properties encompassing the bone that will be able to resist tensile loading. This explains the reason for the positive correlation between sample thickness and suture stiffness. In contrast, suture width was negatively correlated to suture stiffness. It was found in previous studies that a biological adaptation to in vivo quasi-static tensile tests on rat interpremaxillary suture was an increase in suture width and collagen fiber production[1,64]. In another study that applied in vivo tensile forces to rat interparietal suture found an initial decrease in the stiffness but with time, the suture showed adaptations such as collagen fiber production, which increased its stiffness[54]. Although higher suture width will increase the suture material encompassing cranial bones, there should be a collagen fiber structure to effectively resist tensile loading. For an example, unfused cranial sutures in the human skull were reported to have higher suture width and lower stiffness compared to fused/mature sutures with lower suture width[18,23].

This could explain why sutures with higher width have lower stiffness values and were able to displace without going into the larger loads.

Suture LII was not statistically significant in this tensile test. In a previous study, LII was found to be a biological adaptation for swine craniofacial sutures to compressive loading[1,10]. In vivo tensile loading to swine suture reported morphological changes which made the suture less interdigitated[1,10]. Additionally, in previous studies, it was found that higher LII results in a larger bending strength and ability to absorb more energy[14,30]. A study on male wild sheep showed higher interdigitation in the skull sutures were better for stress transmission during head butting in fights between animals[12]. Thus, LII adaptations in internasal sutures might have more significance in their mechanical behavior under different loading conditions such as in vivo compression, in vivo tension, bending and impact loading. This thesis only focused on the internasal suture which had a mean LII of 2.78 with a standard deviation of ± 0.54 across all 42 samples. It is recommended for future studies to test several types of sutures with larger variations in LII to identify the significance of LII in their mechanical behavior.

The position of the sample in the maxilla was not statistically significant in the regression model tested in this thesis. In a previous study on in vivo loading conditions of swine internasal suture during mastication, changes in magnitude of compressive strain in different anatomical regions such as anterior, mid, and posterior regions were observed[10]. The same study reported that the highest LII was at the mid-region, while the posterior region had a lower compressive strain. However, the results were not significant due to a small sample size [10]. This thesis applied ex vivo tensile loading, and as previously mentioned other loading conditions such as in vivo tensile and compression could result in sample position having higher significance. In this thesis, 4-5 samples were dissected from each maxilla from only one anatomical location. Sample position could have an impact with anatomical location, if samples were dissected from various locations of the swine skull, which will result in greater variations to suture mechanical environment [1,10,12,14].

3.5 Conclusion

The objective of this thesis was to identify correlations between swine internasal suture morphology and their mechanical behavior. It expanded on the previous work that found that craniofacial suture mechanical environment affected their morphological adaptations[1,12,14,20,25,30] and studies that applied mechanical loading to bone-suture-bone samples to find relationships between their mechanical properties and cranial suture morphology[8,21–23,41]. This thesis used bone-suture-bone samples from swine internasal sutures and analyzed their 3D morphological and mechanical properties under tensile loading. A multiple regression model was used to discover that the stiffness obtained from the linear region of load vs displacement graph of the swine internasal suture was affected by the suture width and sample thickness with statistical significance. Future work can include other loading conditions such as compression, bending, and impact loading to test for a more comprehensive understanding of mechanical responses and their correlations to internasal suture morphology. Additionally, this thesis considered bulk mechanical properties of the internasal suture samples. FE modeling can be conducted to find the correlations between the mechanical behavior of internasal sutures and their morphological characteristics at a local level.

Chapter 4: Conclusions and Future Work

4.1 Conclusions

The objectives of the thesis were achieved by designing an experiment to derive the mechanical properties of cranial sutures under tensile loading with quasi-static rates at low strain regimes. The 3D morphology of the tested samples was analyzed using μCT imaging techniques. Then, multiple regression was used to find correlations between the mechanical and morphological properties.

The mechanical test consisted of preloading, preconditioning, and tensile testing. Preloading ensured that all samples started with the same starting load and accounted for any minor compressive or tensile loads resulting from loading samples between grips on the Instron E3000 testing machine. During preconditioning the samples undergo cyclic loading between 0.5 - 1 N and ensure that the tensile test starts at a repeatable/ predictable state[61]. Finally, a displacement-controlled tensile test at low strain regimes was performed at a quasi-static rate to obtain the load vs. displacement data from maxilla samples. The load vs. displacement data from the experiments showed nonlinear regions which showed effects from suture material structure at higher loads[23]. Consequently, the initial 10% of the data was removed since this non-linear region occurred in samples at the start of tensile loading. Linear regression was performed with the remaining load vs. displacement data to obtain the gradients, which was a measure of uniaxial stiffness, to be used as the material property in multiple regression analysis.

A 3D image analysis was performed using μCT scans to obtain morphological data, suture width and LII. This analysis was done using a MATLAB script that uses ten image slices through the thickness of each maxilla sample to find the morphological properties in 3D. The minimum, maximum, and mean of these data revealed that for each sample the variation is not significantly large, thus, only the mean value can be used.

The multiple regression model used morphological, positional, and physical properties as independent variables and mechanical data as the dependent variable to find statistical

correlations. Sample physical data included sample thickness and the positional data showed the position of each sample in the maxilla, from posterior to anterior regions. Multiple regression models determined that suture width negatively predicted the gradient, while sample thickness positively predicted the uniaxial stiffness. These findings were consistent with previous studies that reported sutures with higher width having lower stiffness and higher flexibility[1,54]. Sample thickness was a physical characteristic that increases the sample cross-sectional area at the suture, which increases stiffness.

It was concluded that when designing suture models, or analyzing mechanical experiment results, the specific loading conditions need to be considered. Suture material structure also needs to be considered since it will affect their mechanical behavior. Additionally, in the statistical model of internasal suture, using an average value of suture width and LII was sufficient since the bulk mechanical response was used, but to understand the local mechanical behavior, the complex 3D morphology of the suture can be used in an FE model.

4.2 Limitations and Future Work

The mechanical test was conducted on the internasal suture of a swine. The same experiment can be performed on sutures from other areas of the swine skull to observe differences in their adaptations to location and functional environment. It has been suggested in the literature that the internasal suture experienced compression during mastication[23]. This led to adaptations in the arrangement of collagen fibers[23]. A viable way to examine this would be to conduct a study using histology to observe the orientation of fibers and relate these observations to the results of mechanical testing described in this thesis. This will give a comprehensive understanding of the material properties calculated and the nonlinear characteristics observed at the beginning of the load vs displacement data in Appendix B.1.

In the mechanical test, the tensile load was applied in one direction to the bone-suture-bone structure. Previous studies have shown that the direction of loading; parallel/perpendicular to the suture and pressure loading can result in different stress distribution in the suture and strain energies[3,5,6]. In addition, suture mechanical responses

such as energy absorption, bending strength, and stiffness were affected by the morphology[1,2,69]. Thus, to predict these behaviors it is important to investigate multiple sutures from various locations in the skull and loading conditions.

In this thesis, bulk mechanical properties are considered. Additionally, only the average values of morphological data were used since their variation across approximately 5 mm width of a sample is not large enough to include in the multiple regression model. Thus, a FE model can be created to identify the effect of morphology at a local level. Additionally, suitable material properties and collagen fiber directions can be applied to the FE model to get a more comprehensive result of stress and strain distributions under loading.

To improve the multiple regression model, it is necessary to consider a larger population, take samples from various locations, and account for material properties and morphological variations. By taking into account all possible variables, a more accurate statistical model that predicts mechanical properties can be achieved.

References

1. Herring, S. W. Mechanical Influences on Suture Development and Patency. in *Craniofacial Sutures, Frontiers of Oral Biology* 41–56 (S. KARGER AG, 2008). doi:10.1159/000115031.

2. White, H. E., Goswami, A. & Tucker, A. S. The Intertwined Evolution and Development of Sutures and Cranial Morphology. *Front Cell Dev Biol* 9, (2021).

3. Topczewska, J. M., Shoela, R. A., Tomaszewski, J. P., Mirmira, R. B. & Gosain, A. K. The Morphogenesis of Cranial Sutures in Zebrafish. *PLoS One* 11, e0165775 (2016).

4. Slater, B. J. *et al.* Cranial Sutures: A Brief Review. *Plast Reconstr Surg* 121, 170e–178e (2008).

5. Panchal, J. & Uttchin, V. Management of Craniosynostosis. *Plast Reconstr Surg* 111, 2032–2048 (2003).

6. Key, C. A., Aiello, L. C. & Molleson, T. Cranial suture closure and its implications for age estimation. *Int J Osteoarchaeol* 4, 193–207 (1994).

7. Jayaprakash, P. T. & Srinivasan, G. J. Skull sutures: Changing morphology during preadolescent growth and its implications in forensic identification. *Forensic Sci Int* 229, 166.e1-166.e13 (2013).

8. Coats, B. & Margulies, S. S. Material Properties of Human Infant Skull and Suture at High Rates. *J Neurotrauma* 23, 1222–1232 (2006).

9. Beederman, M., Farina, E. M. & Reid, R. R. Molecular basis of cranial suture biology and disease: Osteoblastic and osteoclastic perspectives. *Genes Dis* 1, 120–125 (2014).

10. Rafferty, K. L. & Herring, S. W. Craniofacial sutures: Morphology, growth, and in vivo masticatory strains. *J Morphol* 242, 167–179 (1999).

11. Maloul, A., Fialkov, J. & Whyne, C. M. Characterization of the bending strength of craniofacial sutures. *J Biomech* 46, 912–917 (2013).

12. JASLOW, C. R. Sexual dimorphism of cranial suture complexity in wild sheep (Ovis orientalis). *Zool J Linn Soc* 95, 273–284 (1989).

13. Li, Y., Ortiz, C. & Boyce, M. C. A generalized mechanical model for suture interfaces of arbitrary geometry. *J Mech Phys Solids* **61**, 1144–1167 (2013).

14. Jaslow, C. R. Mechanical properties of cranial sutures. *J Biomech* **23**, 313–321 (1990).

15. Jasinoski, S. C., Reddy, B. D., Louw, K. K. & Chinsamy, A. Mechanics of cranial sutures using the finite element method. *J Biomech* **43**, 3104–3111 (2010).

16. Remesz, R. *et al.* Cranial suture morphometry and mechanical response to loading: 2D vs. 3D assumptions and characterization. *Biomech Model Mechanobiol* **21**, 1251–1265 (2022).

17. Herring, S. W. & Mucci, R. J. In vivo strain in cranial sutures: The zygomatic arch. *J Morphol* **207**, 225–239 (1991).

18. Rafferty, K. L., Herring, S. W. & Marshall, C. D. Biomechanics of the rostrum and the role of facial sutures. *J Morphol* **257**, 33–44 (2003).

19. Herring, S. W. & Teng, S. Strain in the braincase and its sutures during function. *Am J Phys Anthropol* **112**, 575–593 (2000).

20. Sun, Z., Lee, E. & Herring, S. W. Cranial sutures and bones: Growth and fusion in relation to masticatory strain. *Anat Rec A Discov Mol Cell Evol Biol* **276A**, 150–161 (2004).

21. Henderson, J. H., Chang, L. Y., Song, H. M., Longaker, M. T. & Carter, D. R. Age-dependent properties and quasi-static strain in the rat sagittal suture. *J Biomech* **38**, 2294–2301 (2005).

22. Mclaughlin, E., Zhang, Y., Pashley, D., Borke, J. & Yu, J. The Load-Displacement Characteristics of Neonatal Rat Cranial Sutures. *The Cleft Palate-Craniofacial Journal* **37**, 590–595 (2000).

23. Popowics, T. E. & Herring, S. W. Load transmission in the nasofrontal suture of the pig, Sus scrofa. *J Biomech* **40**, 837–844 (2007).

24. Moore, A. W., Anderson, B., Das, K. & Wong, W. K. Combining Multiple Signals for Biosurveillance. in *Handbook of Biosurveillance* (2006). doi:10.1016/B978-012369378-5/50017-X.

25. Khonsari, R. H. *et al.* A mathematical model for mechanotransduction at the early steps of suture formation. *Proceedings of the Royal Society B: Biological Sciences* **280**, 20122670 (2013).

26. Roth, D. M., Souter, K. & Graf, D. Craniofacial sutures: Signaling centres integrating mechanosensation, cell signaling, and cell differentiation. *Eur J Cell Biol* **101**, 151258 (2022).

27. Cardozo, C. P. Mechanotransduction: Overview. in *Encyclopedia of Bone Biology* 217 (Elsevier, 2020). doi:10.1016/B978-0-12-801238-3.62233-X.

28. Thomas, S. & Jaganathan, B. G. Signaling network regulating osteogenesis in mesenchymal stem cells. *J Cell Commun Signal* **16**, 47–61 (2022).

29. Naroda, Y. *et al.* Noise-induced scaling in skull suture interdigitation. *PLoS One* **15**, e0235802 (2020).

30. Zhang, Z. Q. & Yang, J. L. Biomechanical Dynamics of Cranial Sutures during Simulated Impulsive Loading. *Appl Bionics Biomech* **2015**, 1–11 (2015).

31. Byron, C. D. *et al.* Effects of increased muscle mass on mouse sagittal suture morphology and mechanics. *Anat Rec A Discov Mol Cell Evol Biol* **279A**, 676–684 (2004).

32. Miura, T. *et al.* Mechanism of skull suture maintenance and interdigitation. *J Anat* **215**, 642–655 (2009).

33. Byron, C. D. Role of the osteoclast in cranial suture waveform patterning. *Anat Rec A Discov Mol Cell Evol Biol* **288A**, 552–563 (2006).

34. Maloul, A., Fialkov, J., Wagner, D. & Whyne, C. M. Characterization of craniofacial sutures using the finite element method. *J Biomech* (2014) doi:10.1016/j.jbiomech.2013.09.009.

35. Bright, J. A. & Rayfield, E. J. The Response of Cranial Biomechanical Finite Element Models to Variations in Mesh Density. *Anat Rec* **294**, 610–620 (2011).

36. Bright, J. A. The Importance of Craniofacial Sutures in Biomechanical Finite Element Models of the Domestic Pig. *PLoS One* **7**, e31769 (2012).

37. Moazen, M. *et al.* Mechanical loading of cranial joints minimizes the craniofacial phenotype in Crouzon syndrome. *Not available* (2021) doi:10.1101/2021.08.31.458360.

38. Markey, M. J. & Marshall, C. R. Linking form and function of the fibrous joints in the skull: A new quantification scheme for cranial sutures using the extant fish *Polypterus endlicherii*. *J Morphol* **268**, 89–102 (2007).

39. Liu, L. *et al.* The effects of morphological irregularity on the mechanical behavior of interdigitated biological sutures under tension. *J Biomech* **58**, 71–78 (2017).

40. White, H. E., Clavel, J., Tucker, A. S. & Goswami, A. A comparison of metrics for quantifying cranial suture complexity. *J R Soc Interface* **17**, 20200476 (2020).

41. Hubbard, R. P., Melvin, J. W. & Barodawala, I. T. Flexure of cranial sutures. *J Biomech* **4**, 491–496 (1971).

42. Chen, Y. Mechanical Properties of Cranial Bones and Sutures in 1–2-Year-Old Infants. *Medical Science Monitor* **20**, 1808–1813 (2014).

43. Pritchard, J. J., Scott, J. H. & Girgis, F. G. The structure and development of cranial and facial sutures. *J Anat* (1956).

44. Soliman, L., Ahn, S., Hunt, V., Sobti, N. & Woo, A. S. Gaining Closure: Do Cranial Sutures Fuse at Reported Age Ranges? *Plast Reconstr Surg Glob Open* **11**, e5013 (2023).

45. Zhai, X., Nauman, E. A., Moryl, D., Lycke, R. & Chen, W. W. The effects of loading-direction and strain-rate on the mechanical behaviors of human frontal skull bone. *J Mech Behav Biomed Mater* **103**, 103597 (2020).

46. Adanty, K. *et al.* The effect of morphometric and geometric indices of the human calvarium on mechanical response. *Clinical Biomechanics* **107**, 106012 (2023).

47. Shahar, R., Kraus, S., Monsonego-Ornan, E. & Fratzl, P. Mechanical Function of a Complex Three-dimensional Suture Joining the Bony Elements in the Shell of the Red-eared Slider Turtle. *MRS Proceedings* **1187**, 1187-KK01-05 (2009).

48. Motherway, J. A., Verschueren, P., Van der Perre, G., Vander Sloten, J. & Gilchrist, M. D. The mechanical properties of cranial bone: The effect of loading rate and cranial sampling position. *J Biomech* **42**, 2129–2135 (2009).

49. Sharp, A. C. *et al.* Assessment of the mechanical role of cranial sutures in the mammalian skull: Computational biomechanical modelling of the rat skull. *J Morphol* **284**, (2023).

50. Adamski, K. N. *et al.* Pediatric Coronal Suture Fiber Alignment and the Effect of Interdigitation on Coronal Suture Mechanical Properties. *Ann Biomed Eng* **43**, 2101–2111 (2015).

51. Moazen, M. *et al.* Assessment of the role of sutures in a lizard skull: a computer modelling study. *Proceedings of the Royal Society B: Biological Sciences* **276**, 39–46 (2009).

52. Wang, Q. *et al.* The Role of the Sutures in Biomechanical Dynamic Simulation of a Macaque Cranial Finite Element Model: Implications for the Evolution of Craniofacial Form. *Anat Rec* **295**, 278–288 (2012).

53. Soh, S. H., Rafferty, K. & Herring, S. Cyclic loading effects on craniofacial strain and sutural growth in pigs. *American Journal of Orthodontics and Dentofacial Orthopedics* **154**, 270–282 (2018).

54. Tanaka, E., Miyawaki, Y., del Pozo, R. & Tanne, K. Changes in the biomechanical properties of the rat interparietal suture incident to continuous tensile force application. *Arch Oral Biol* **45**, 1059–1064 (2000).

55. Fuhrer, R. S., Romanyk, D. L. & Carey, J. P. A comparative finite element analysis of maxillary expansion with and without midpalatal suture viscoelasticity using a representative skeletal geometry. *Sci Rep* **9**, 8476 (2019).

56. Katsianou, M. A., Adamopoulos, C., Vastardis, H. & Basdra, E. K. Signaling mechanisms implicated in cranial sutures pathophysiology: Craniosynostosis. *BBA Clin* **6**, 165–176 (2016).

57. Shibazaki-Yorozuya, R., Wang, Q., Dechow, P. C., Maki, K. & Opperman, L. A. Changes in Biomechanical Strain and Morphology of Rat Calvarial Sutures and Bone After Tgf-β3 Inhibition of Posterior Interfrontal Suture Fusion. *Anat Rec* **295**, 928–938 (2012).

58. Houg, K. P. *et al.* Experimental repeatability, sensitivity, and reproducibility of force and strain measurements from within the periodontal ligament space during ex vivo swine tooth loading. *J Mech Behav Biomed Mater* **120**, 104562 (2021).

59. Abramowitch, S. D., Woo, S. L.-Y., Clineff, T. D. & Debski, R. E. An Evaluation of the Quasi-Linear Viscoelastic Properties of the Healing Medial Collateral Ligament in a Goat Model. *Ann Biomed Eng* **32**, 329–335 (2004).

60. Carew, E. O., Barber, J. E. & Vesely, I. Role of Preconditioning and Recovery Time in Repeated Testing of Aortic Valve Tissues: Validation Through Quasilinear Viscoelastic Theory. *Ann Biomed Eng* **28**, 1093–1100 (2000).

61. Fung, Y. C. & Skalak, R. Biomechanics: Mechanical Properties of Living Tissues. *J Biomech Eng* **103**, (1981).

62. Lee, D. T. Medial Axis Transformation of a Planar Shape. *IEEE Trans Pattern Anal Mach Intell* **PAMI-4**, (1982).

63. Mongomery, D. C. Montgomery: Design and Analysis of Experiments. *John Willy & Sons* Preprint at (2017).

64. Southard, K. A. & Forbes, D. P. The effects of force magnitude on a sutural model: A quantitative approach. *American Journal of Orthodontics and Dentofacial Orthopedics* **93**, 460–466 (1988).

65. Cohen, J. Statistical power analysis for the behavioural sciences. Hillside. *NJ: Lawrence Earlbaum Associates* Preprint at (1988).

66. Paul, R. K. Multicollinearity: Causes, effects and remedies. (2006).

67. Bianco, G., Levy, A. M., Grytz, R. & Fazio, M. A. Effect of different preconditioning protocols on the viscoelastic inflation response of the posterior sclera. *Acta Biomater* **128**, 332–345 (2021).

68. Goss-Sampson, D. M. A. *Statistical Analysis in JASP - A Guide for Students (JASP) v0.16(2022)*. *Mark A Goss-Sampson* vol. 4 (2022).

69. Jiang, M. *et al.* Clamping soft biologic tissues for uniaxial tensile testing: A brief survey of current methods and development of a novel clamping mechanism. *J Mech Behav Biomed Mater* **103**, 103503 (2020).

70. Robi, K., Jakob, N., Matevz, K. & Matjaz, V. The Physiology of Sports Injuries and Repair Processes. in *Current Issues in Sports and Exercise Medicine* (InTech, 2013). doi:10.5772/54234.

Appendix A : Sample Dimensions

A.1 Sample Dimensions

A total of 42 samples were taken from nine maxillae and their physical dimensions are listed below. The width of each sample was controlled to approximately 5 mm during dissection, while the thickness refers to the thickness of the nasal bone. Additionally, the position of each sample in every maxilla was measured from the posterior to the anterior region.

Table 5: Sample Dimensions

Swine Maxilla	Sample Number from Posterior to Anterior Region	Number of Samples	Sample Width (mm)	Sample Thickness (mm)	Sample Position in the Maxilla (mm)
1	1	4	6.09	7.56	3.045
	2		4.66	6.09	8.42
	3		6.28	6.00	13.89
	4		5.66	5.32	19.86
2	1	5	5.00	8.97	2.5
	2		5.12	6.44	7.56
	3		5.43	6.00	12.84
	4		4.92	5.26	18.01
	5		4.85	5.60	22.90

Swine Maxilla	Sample Number from Posterior to Anterior Region	Number of Samples	Sample Width (mm)	Sample Thickness (mm)	Sample Position in the Maxilla (mm)
3	1	5	5.76	7.82	2.88
	2		5.65	7.04	8.59
	3		5.40	6.11	14.11
	4		5.23	6.09	19.43
	5		5.06	6.04	24.57
4	1	6	4.98	8.03	2.49
	2		4.42	7.37	7.19
	3		5.09	6.22	11.95
	4		5.01	5.83	17.00
	5		4.24	6.33	21.62
	6		5.45	6.25	26.47
5	1	5	5.46	6.32	2.73
	2		4.94	5.29	7.93
	3		4.90	5.37	12.85
	4		4.71	4.66	17.66
	5		4.18	5.03	22.10
6	1	4	5.70	7.45	2.85
	2		4.67	6.83	8.04
	3		5.01	5.96	12.88
	4		5.03	4.85	17.90

Swine Maxilla	Sample Number from Posterior to Anterior Region	Number of Samples	Sample Width (mm)	Sample Thickness (mm)	Sample Position in the Maxilla (mm)
7	1	4	4.93	7.80	2.465
	2		4.37	7.23	7.12
	3		4.22	6.43	11.41
	4		4.52	5.78	15.78
8	1	5	3.82	7.93	1.91
	2		4.91	6.46	6.28
	3		4.81	5.64	11.14
	4		4.16	5.13	15.62
	5		5.21	5.41	20.31
9	1	5	4.48	9.37	2.24
	2		5.18	7.17	7.07
	3		5.23	5.48	12.28
	4		4.48	5.86	17.13
	5		5.36	5.43	22.05

Appendix B: Mechanical Testing Data

B.1 Load vs. Displacement Data

This section shows graphs of load (N) vs displacement (mm) of the tensile test that was conducted after preloading and preconditioning.

Figure 20: Swine 1 - Load vs. Displacement Data

Figure 21: Swine 2 - Load vs. Displacement Data
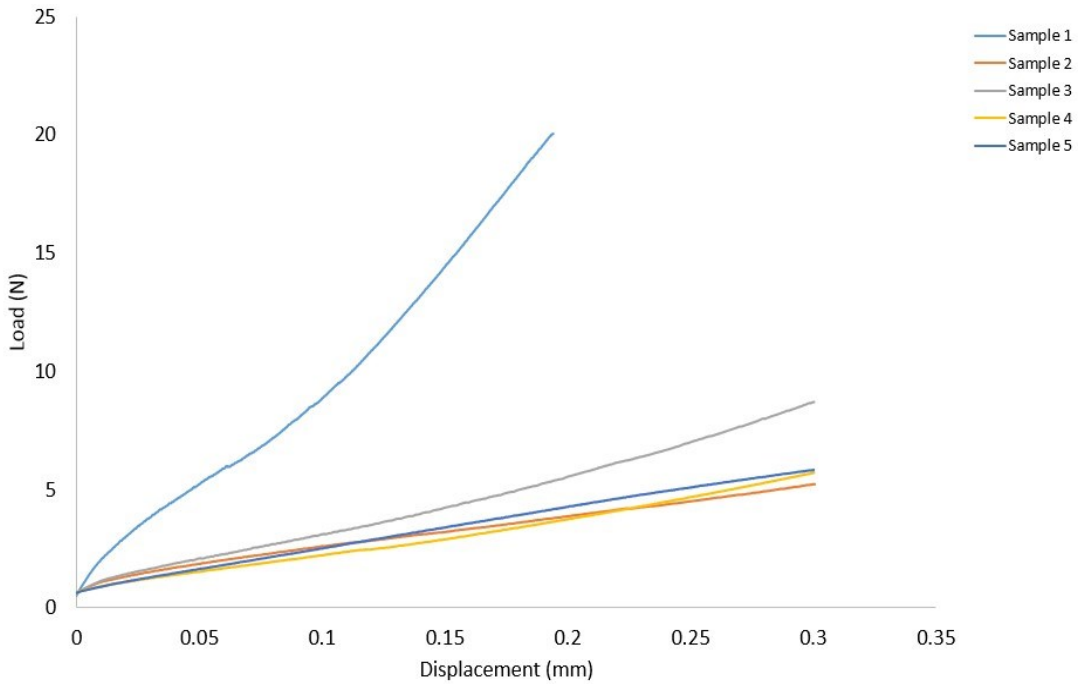
Figure 22: Swine 3 - Load vs. Displacement Data
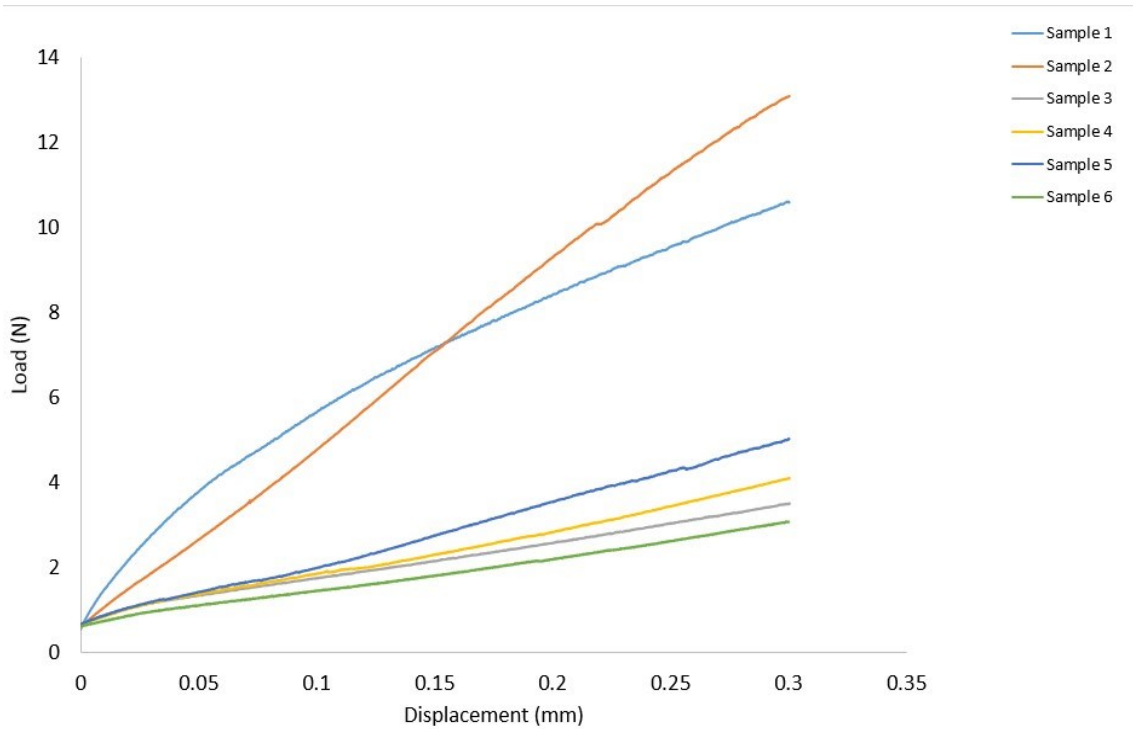
Figure 23: Swine 4 - Load vs. Displacement Data
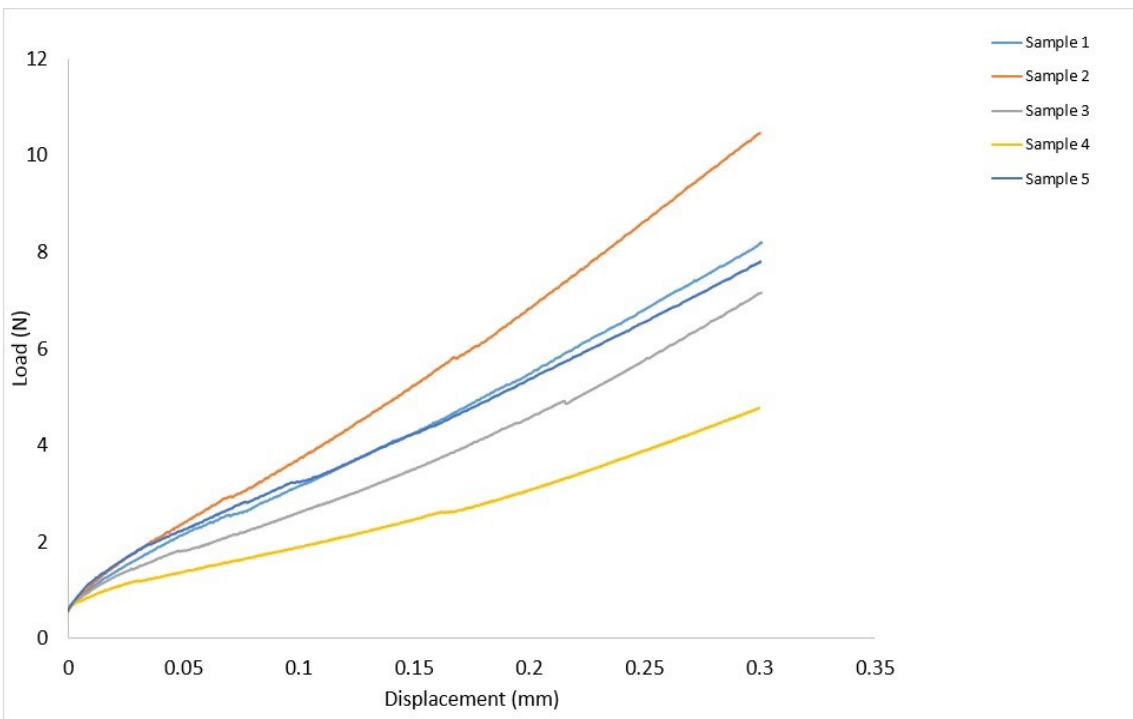
Figure 24: Swine 5 - Load vs. Displacement Data

60

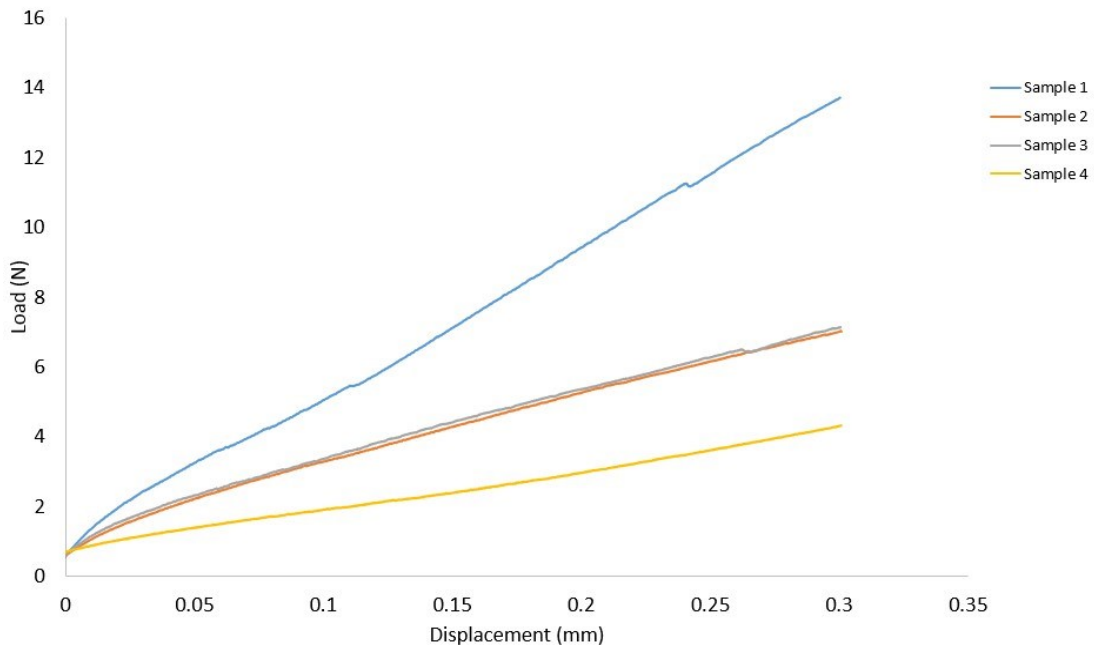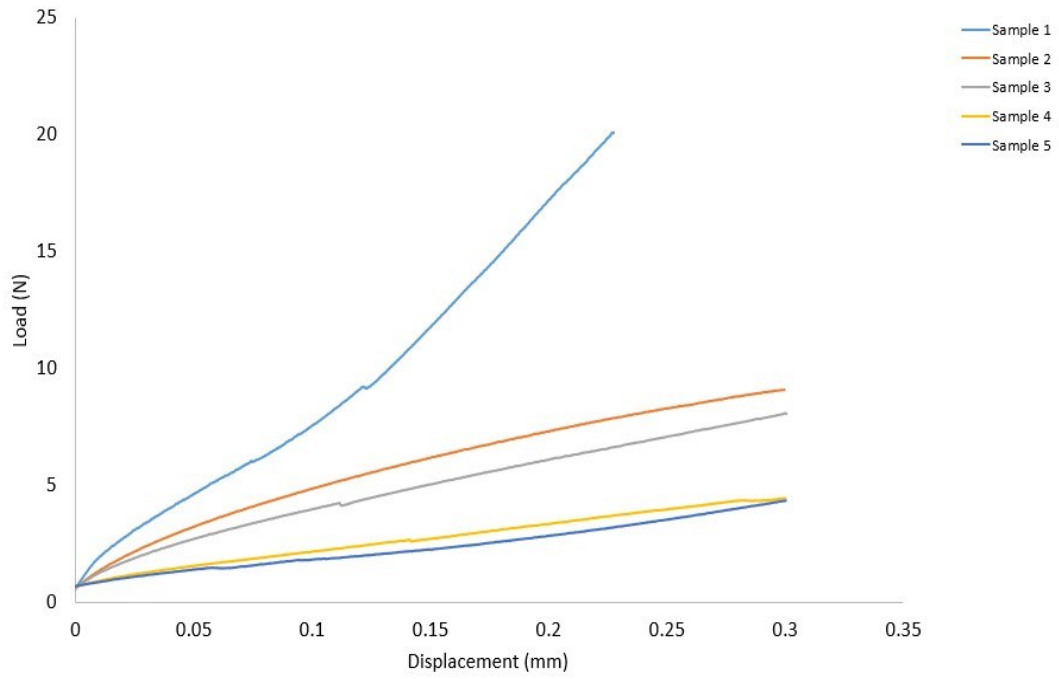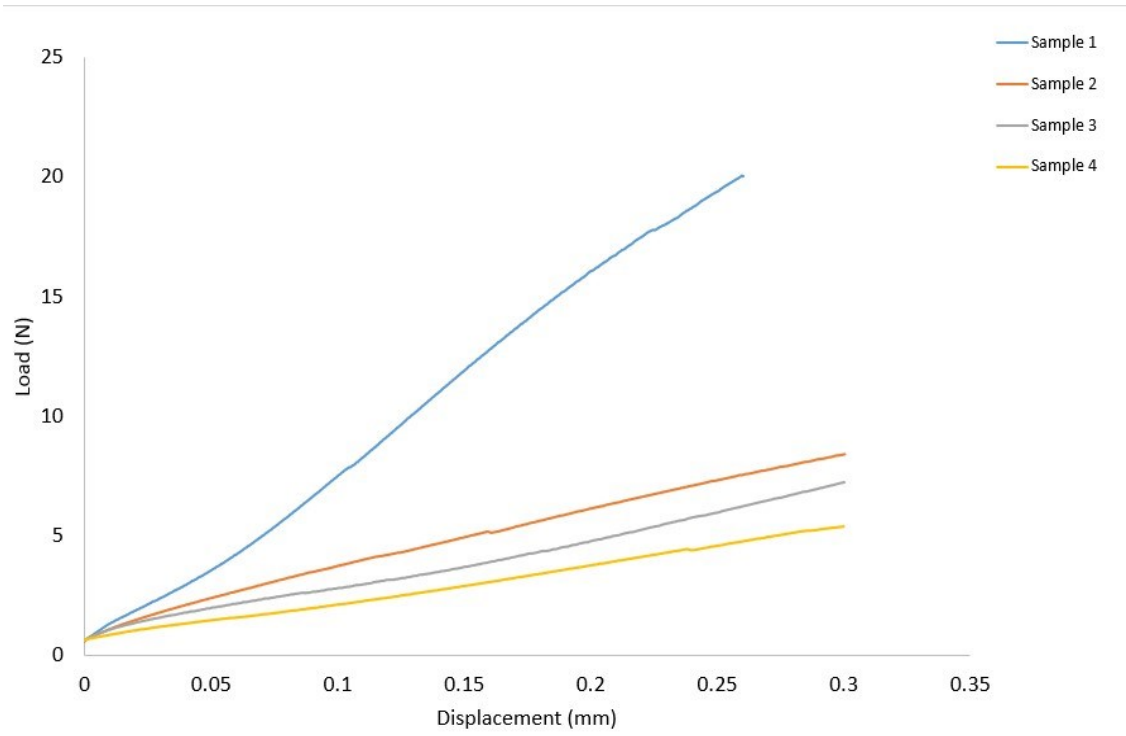*Figure 25: Swine 6 - Load vs. Displacement Data*
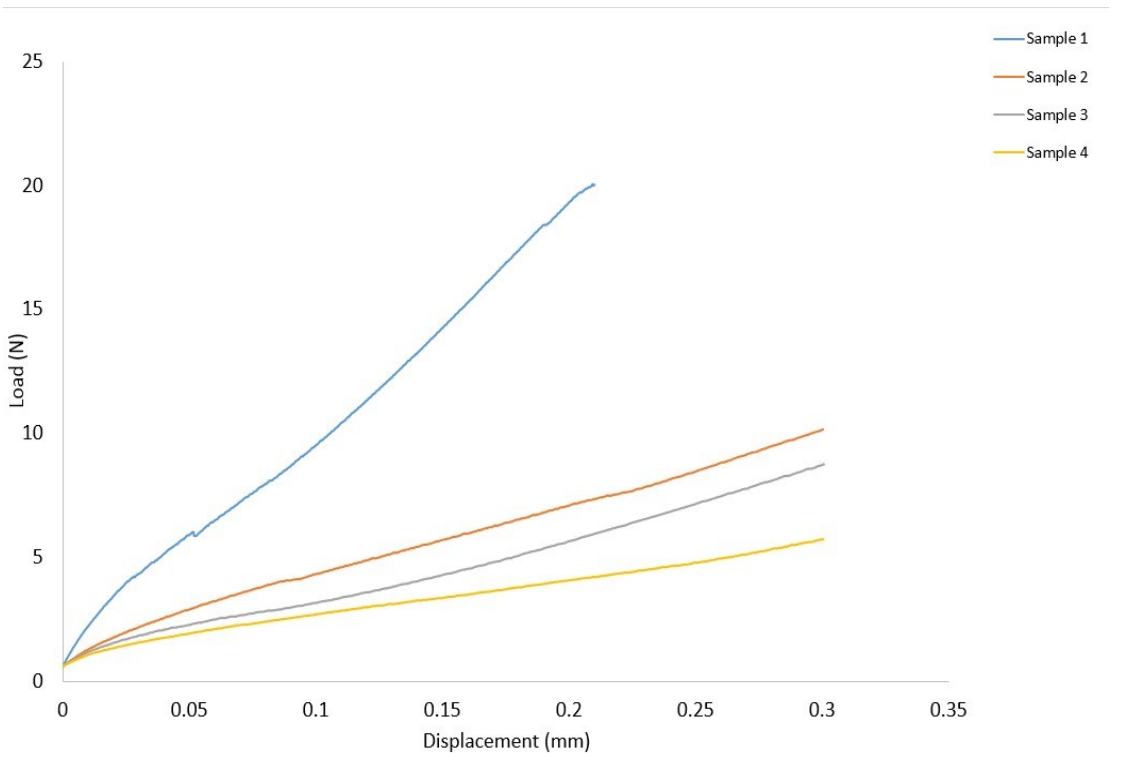
Figure 26: Swine 7 - Load vs. Displacement Data
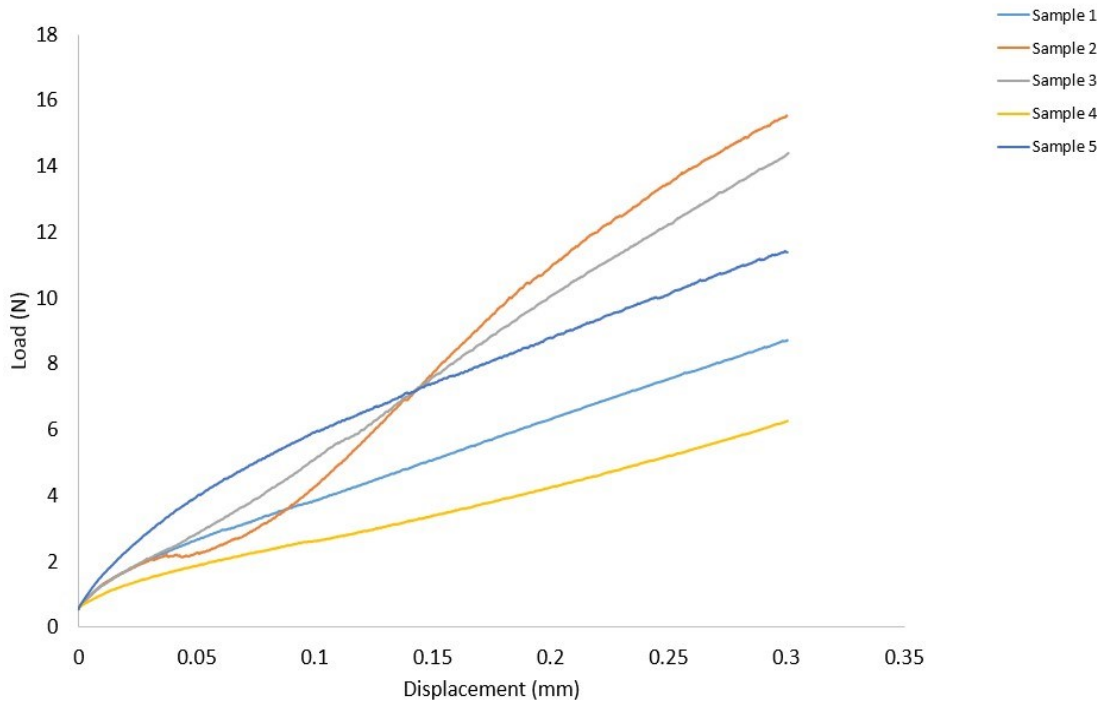
Figure 27: Swine 8 - Load vs. Displacement Data
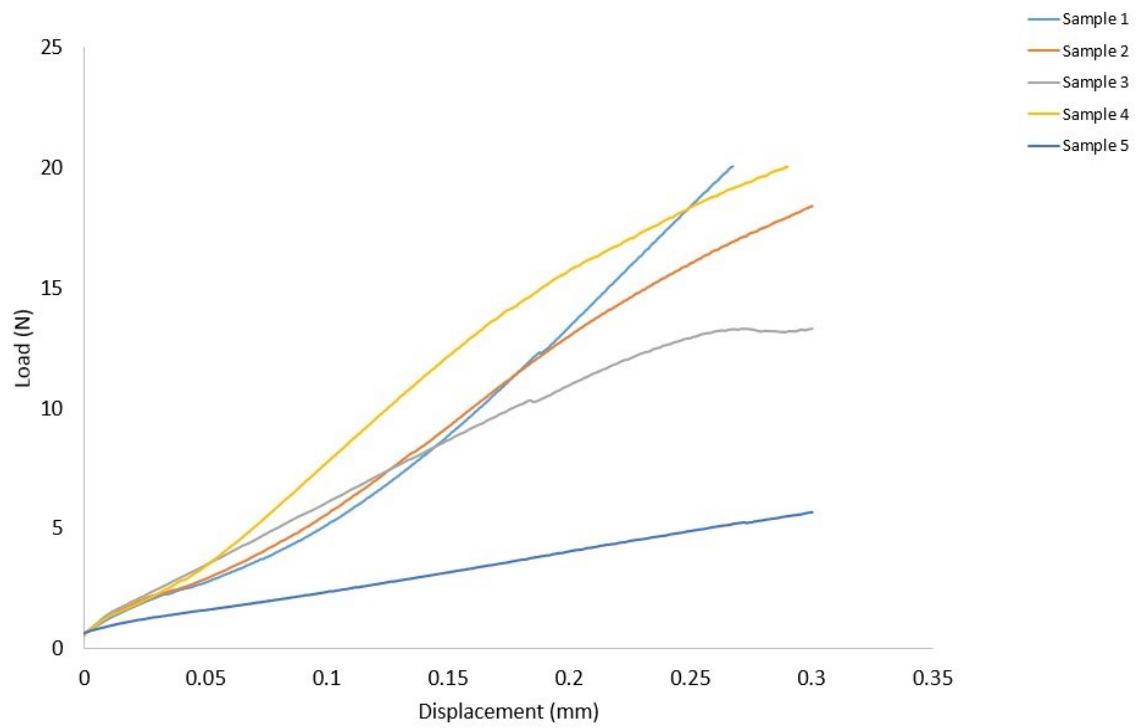
Figure 28: Swine 9 - Load vs. Displacement Data

B.2 Mechanical Property: Gradient of Load vs. Displacement Data

This section displays graphs of the relationship between load (N) and displacement (mm) for all samples, separated by swine maxillae. To account for the nonlinear region at the beginning, which may have been caused by the suture material structure[23], the initial 10% of the tensile test data was removed[22,23,70]. After that, a linear regression model was used to determine the gradient of the load (N) vs displacement (mm) data.
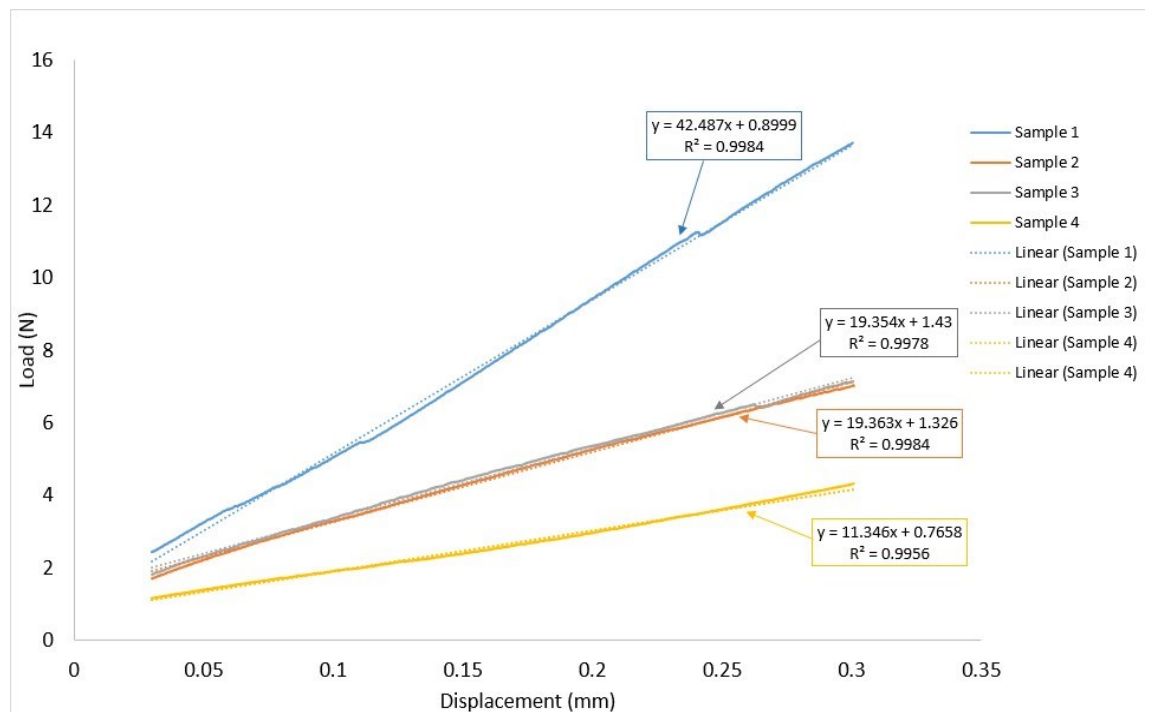
Figure 29: Swine 1 - Linear Regression
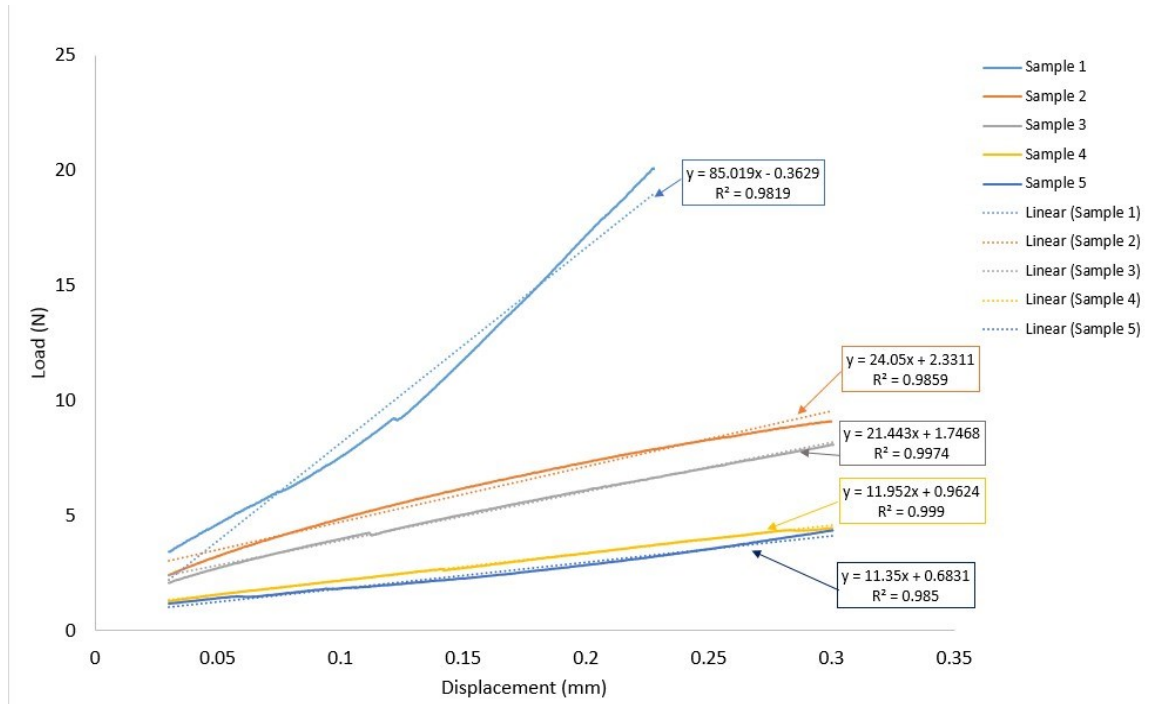
Figure 30: Swine 2 - Linear Regression
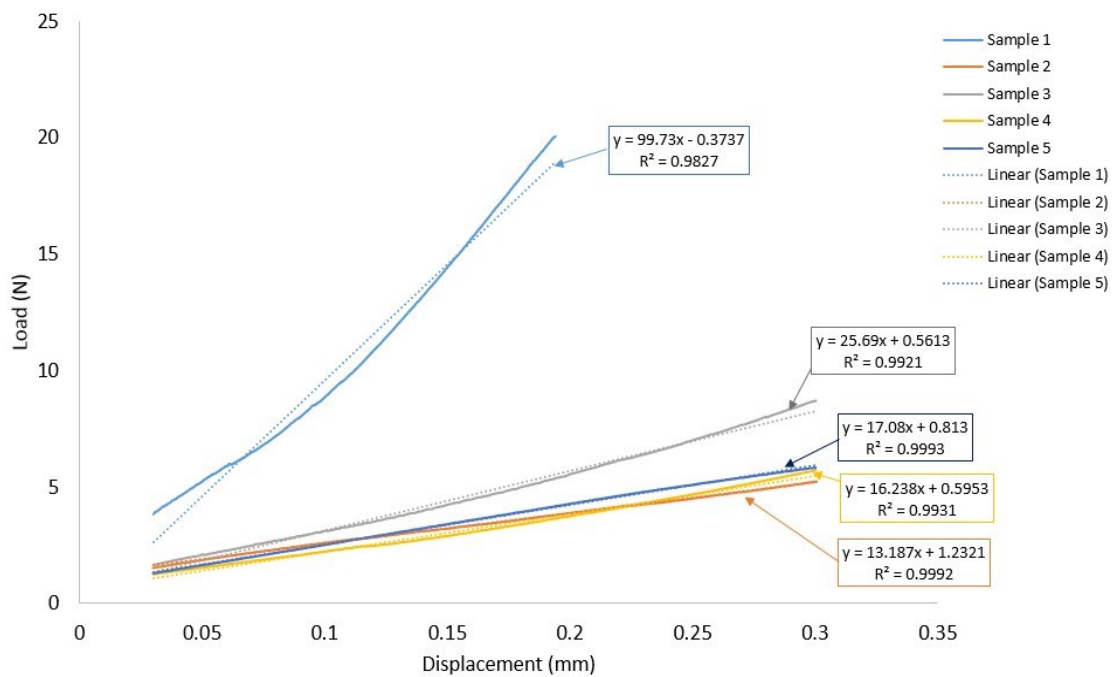
Figure 31: Swine 3 - Linear Regression

64
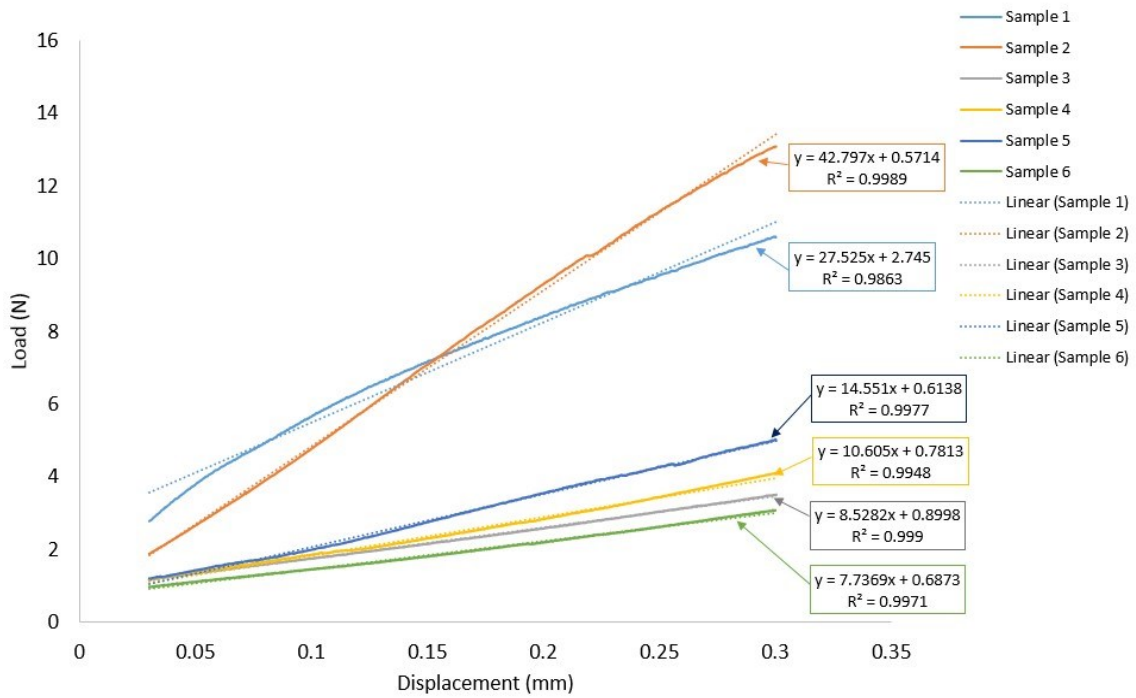
Figure 32: Swine 4 - Linear Regression
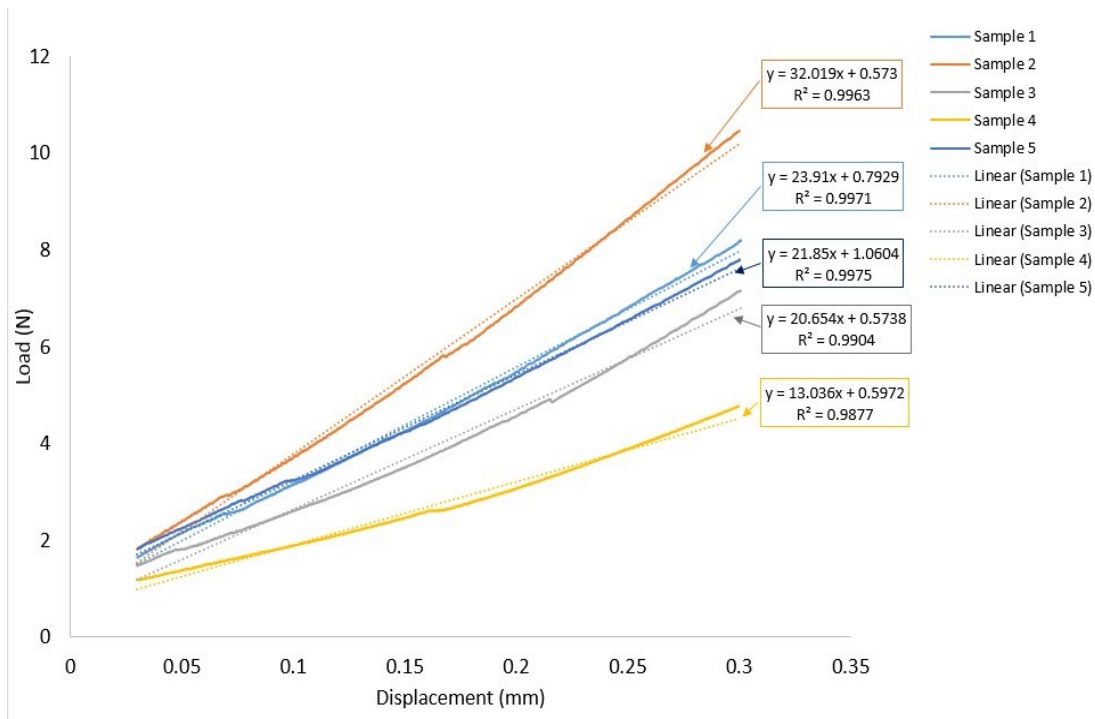
Figure 33: Swine 5 - Linear Regression
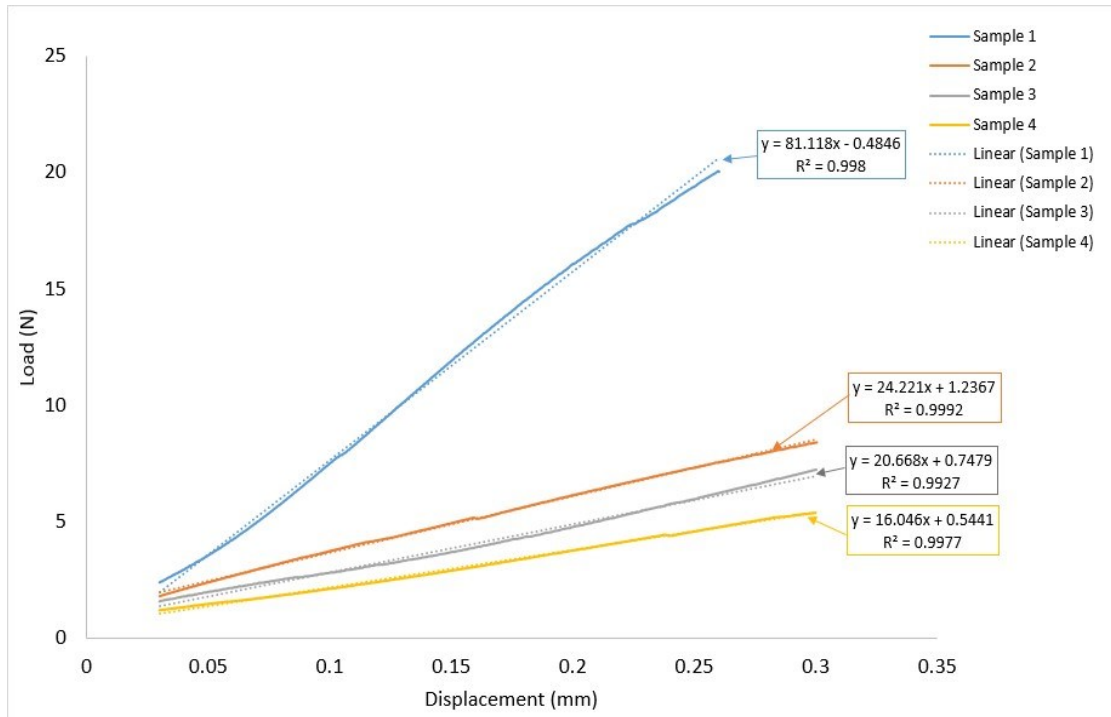
Figure 34: Swine 6 - Linear Regression
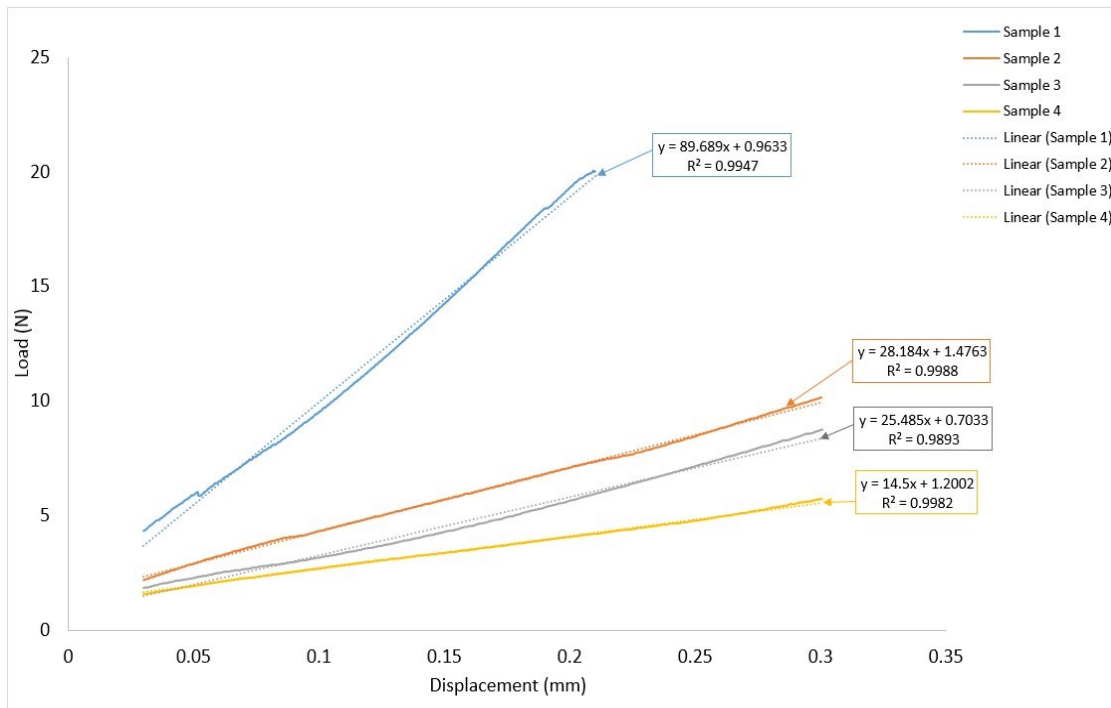
Figure 35: Swine 7 - Linear Regression
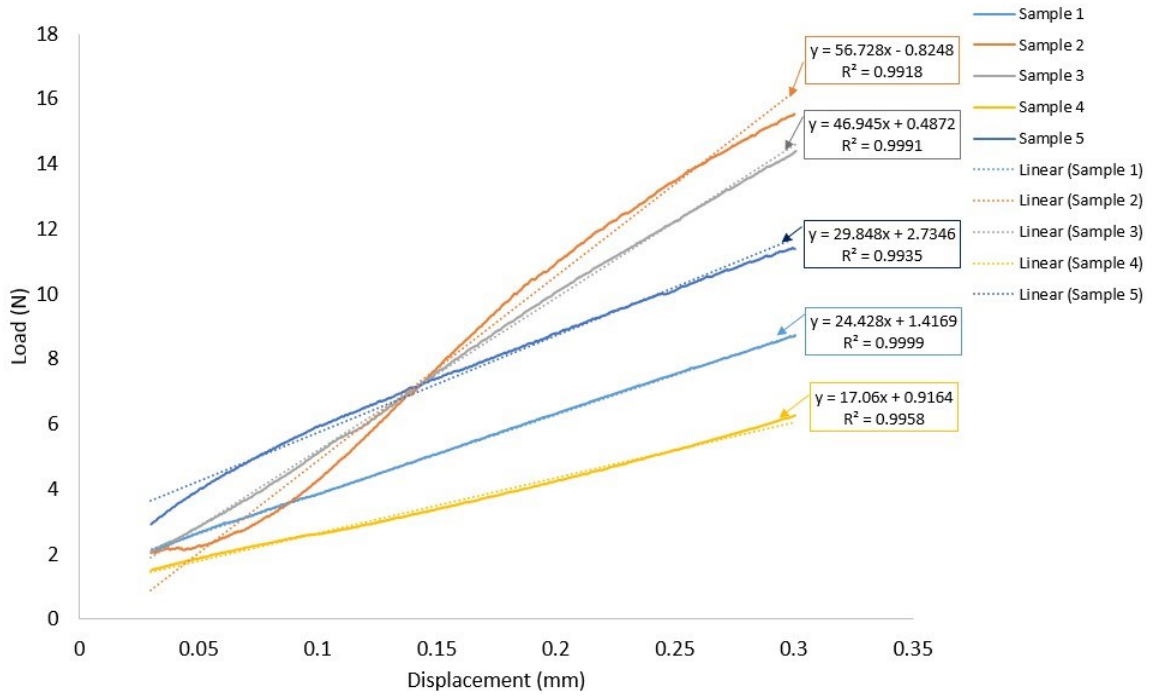
Figure 36: Swine 8 - Linear Regression
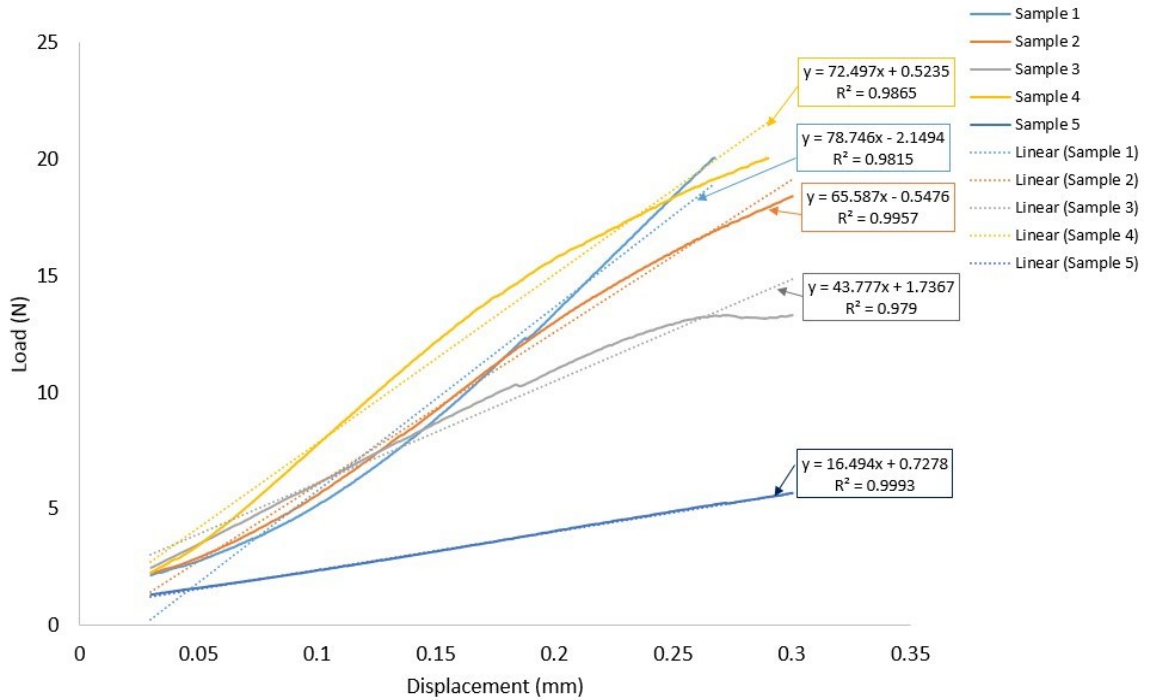
Figure 37: Swine 9 - Linear Regression

Appendix C: MATLAB Scripts

C.1 Initial Image Processing

This MATLAB script processes all μCT data to retrieve morphological information.

```matlab
% Multiple Scan Analysis

%----- Initializing steps -----
% Clean up clc; close all; clear all; workspace; % Display the
workspace panel. fontSize = 20;

% USER INPUTS:
% STRUCTURING ELEMENT: NOTE SHOULD BE APPROXIMATE SIZE AS
    OBJECTS se = strel('disk',2);
% SENSITIVITY FACTOR FOR ADAPTIVE THRESHOLDING sens = 0.65;
resolution = 8.9029;          % CT SCAN RESOLUTION, 1 pixel =
    8.9029 um resize = 2; % Intervals between adjacent scans
sampled Data = imageDatastore('Sample 1'); % DATA INPUT scanData
= struct();


crop = [900,800,800,600]; % Change for every unique suture % This
puts the suture of interest into titles suture = 'BML-XX,
SUTURE_NAME'; suturesave = 'BMLXX_SUTURENAME_';

% Ensuring that user has necessary apps % (Image Processing Toolbox
is required) hasIPT = license('test', 'image_toolbox'); if ~hasIPT
% User does not have the toolbox installed.
message = sprintf('you do not have  the Image Processing
Toolbox');
```

68

```matlab
reply = questdlg(message, 'Toolbox missing', 'Yes', 'No',
    'Yes'); if strcmpi(reply, 'No') % User said No, so exit.
return; end end


%%%% SEGMENTATION

% Creating loop to handle the dataset.
for i=1:(length(Data.Files))
% Extracting file number from the Data input % INPUTS REQUIRED:
% Look at the file name of string and input the string before and
after % the marker/file number before = "SUTURE IDENTIFYING
TEXT"; after = ".bmp"; scanData.ID{i} =
char(extractBetween(Data.Files{i},before, after));
scanData.FileName{i} = join(['Processed',scanData.ID{i},'.
    tif']);

% Cropping the image
scanData.Cropped{i} = imcrop(imread(Data.Files{i}),crop);
% figure, imshow(scanData.Cropped{i})
%  title(['Cropped Image of ',suture,num2str( scanData.ID{i})])

% Equalizing the GSV histograms so consistant adjustments will
    work
scanData.Equalized{i} = histeq(scanData.Cropped{i},256); %
     figure, imshow(scanData.Equalized{i})
%  title(['Histogram Equalization ',suture,num2str(
    scanData.ID{i})])

% Adjust the image intesity values to increase contrast
scanData.Adjust{i} = scanData.Equalized{i}; %    figure,
imshow(scanData.Adjust{i})
%           title(['Adjusted Image of ',suture,scanData.ID{i
}])
```

69

```matlab
% Binarizing the adjusted image
scanData.BW{i}=imbinarize(scanData.Adjust{i},'adaptive',...
'Sensitivity',sens); figure, imshow(scanData.BW{i})
%            title(['Binary Image of ',suture,scanData.ID{i
}])

% Filling the holes in the image scanData.Filled{i} =
bwareaopen(scanData.BW{i}, 30, 4); %  figure,
imshow(scanData.Filled{i})
%            title(['Filled Image of ',suture,scanData.ID{i
}])

%    % Morphologically opening image (sequential eriosion and
    dilation)
scanData.Opened{i} = imopen(~scanData.Filled{i},se);
%            figure, imshow(scanData.Opened{i})
%             title(['Morphologically Opened ',suture,scanData
.ID{i}])

% Filling the holes in the image scanData.Filled2{i} =
bwareaopen(scanData.Opened{i}, 30,
8); figure, imshow(scanData.Filled2{i})
%             title (['Filled Image of Opened ',suture,scanData
.ID{i}])


%
%%%%%%%%%%%%%%%%%%%%%%%%%%%%%%%%%%%%%%%%%%%%%%%%%%%%%%%%%%%%%%

% BURNING WHITE REGION
% Display images to prepare for ease of use burnedImage =
scanData.Filled2{i}; OGImage = scanData.Cropped{i}; subplot(2, 2,
1); imshow(OGImage); title('Original Image', 'FontSize',
fontSize); subplot(2, 2, 2); imshow(burnedImage); current=i;
```

```matlab
total=length(Data.Files);
title(['White',num2str(current),'/',num2str(total)],'...
    FontSize',fontSize); subplot(2, 2, 4); imshow(burnedImage);
title('Original Image with regions burned', 'FontSize', fontSize);
set(gcf, 'units','normalized','outerposition',[0 0 1 1]);
% Maximize figure.
set(gcf,'name','Manual Suture Segmentation','numbertitle', 'off')

%----- Burn region into image -----
% Create a binary image for all the regions we will draw.
cumulativeBinaryImage = false(size(burnedImage)); subplot(2, 2,
3); imshow(burnedImage); title('Binary Image', 'FontSize',
fontSize);
% Create region mask, h, as an ROI object over the image.
axis on; again = true; regionCount = 0; while again &&
regionCount < 20
promptMessage = sprintf('Draw region #%d,\nor Quit?',
    regionCount+1);
titleBarCaption = 'Continue?';
button=questdlg(promptMessage,titleBarCaption,'Draw','...
    Quit','Draw'); if strcmpi(button, 'Quit') break;
end
regionCount = regionCount + 1; subplot(2, 2, 2);

% Ask user to draw freehand mask.

% uiwait(msgbox(message)); hFH = imfreehand(); % Actual line of
 code to do the drawing.
% Create a binary image ("mask") from the ROI object.
singleRegionBinaryImage = hFH.createMask(); xy = hFH.getPosition;

caption = sprintf('DRAW.Original Image with %d regions',
    regionCount);
title(caption, 'FontSize', fontSize);
```

71

```matlab
    % OR it in to the "all regions" binary image mask we' re
building up. cumulativeBinaryImage = cumulativeBinaryImage|
singleRegionBinaryImage; % Display the regions mask. subplot(2,
2, 3); imshow(cumulativeBinaryImage); caption = sprintf('Binary
mask of the %d regions', regionCount);
title(caption, 'FontSize', fontSize);

% Burn region into image by setting it to 255 wherever the mask
    is true.
burnedImage(cumulativeBinaryImage) = 255;
% Display the image with the "burned in" region. subplot(2, 2, 4);
cla; imshow(burnedImage);
caption = sprintf('New image with %d regions burned',
    regionCount);
title(caption, 'FontSize', fontSize);
end
% Saving the Segmented Images
scanData.PreSegmented{i}=burnedImage;

%%%%%%%%%
% BURNING BLACK REGION
% Display images to prepare for ease of use burnedImage =
scanData.PreSegmented{i};    OGImage    =    scanData.Cropped{i};
subplot(2,  2,  1);  imshow(OGImage);  title('Original  Image',
'FontSize',  fontSize);  subplot(2,  2,  2);  imshow(burnedImage);
current=i;                           total=length(Data.Files);
title(['BurnBlackRegion',num2str(current),'/',num2str(
total)],...
    'FontSize',fontSize); subplot(2, 2, 4); imshow(burnedImage);
title('Original Image with regions burned ','FontSize', fontSize);
set(gcf,'units','normalized','outerposition',[0 0 1 1]);% Maximize
figure.
set(gcf,'name','Manual Suture Segmentation','numbertitle', 'off')
```

```matlab
%----- Burn region into image -----
% Create a binary image for all the regions we will draw.
cumulativeBinaryImage = false(size(burnedImage)); subplot(2, 2,
3); imshow(burnedImage); title('Binary Image', 'FontSize',
fontSize);
% Create region mask, h, as an ROI object over the second image.
axis on; again = true; regionCount = 0; while again &&
regionCount < 20 promptMessage=sprintf('Draw region #%d ,\nor
Quit?', regionCount+1);
titleBarCaption = 'Continue?';
button = questdlg(promptMessage,titleBarCaption,'Draw','
   Quit','Draw'); if strcmpi(button, 'Quit') break;
end regionCount = regionCount + 1; subplot(2, 2, 2);

% Ask user to draw freehand mask.

% uiwait(msgbox(message)); hFH = imfreehand(); % Actual line of
 code to do the drawing.
% Create a binary image ("mask") from the ROI object.
singleRegionBinaryImage = hFH.createMask(); xy = hFH.getPosition;

caption = sprintf('DRAW.Original Image with %d regions',
   regionCount);
title(caption, 'FontSize', fontSize);

   % OR it in to the "all regions" binary image mask we' re
building up. cumulativeBinaryImage = cumulativeBinaryImage|
singleRegionBinaryImage;
% Display the regions mask.
 subplot(2, 2, 3); imshow(cumulativeBinaryImage); caption
 = sprintf('Binary mask of the %d regions',
   regionCount); title(caption, 'FontSize', fontSize);
```

```matlab
 region into image by setting it to 0 wherever mask is
 true.
 burnedImage(cumulativeBinaryImage) = 0;
 % Display   the   image   with   the   "burned   in"   region.
 subplot(2, 2, 4); cla; imshow(burnedImage);
caption = sprintf('New image with %d regions', regionCount
); title(caption, 'FontSize', fontSize);
end

% Saving the Segmented Images
scanData.ManualSegmented{i}=burnedImage; figure,
imshow(scanData.ManualSegmented{i}) title(['Post-Segmentation
',suture,scanData.ID{i}])

% Isolating the largest area
scanData.FinalArea{i}=bwpropfilt(scanData.ManualSegmented{
i},'Area',1);
%           figure, imshow(scanData.FinalArea{i})
% title(['Final Area ',suture,scanData.ID{i}]) % Filling potential
stray   pixels   within   the   ROI:   scanData.SegSmooth{i}   =
imfill(scanData.FinalArea{i},' holes');
%           figure, imshow(scanData.SegSmooth{i})
%            title(['Fully Segmented ',suture,scanData.ID{i
   }]) end
```

C.2 Suture Analysis

This code loops through all morphological data, records, and summarizes them.

```matlab
% Looping though the segmented files
for i=1:(length(Data.Files))
    [scanData.Center{i},scanData.Width{i}]=
        SutureAnalysisMAClosestDist(...
```

```matlab
            scanData.SegSmooth{i});
    end

    h=(length(Data.Files))*resize*resolution;% Setting the
        height to maximum
    fig=figure; for i=1:(length(Data.Files))
    scanData.h_LII{i}=h;
    height=h*ones(length(scanData.Center{i}(:,1)),1);
    plot3(resize*resolution*scanData.Center{i}(:,1),...
    (crop(1,4)*resolution*resize)-resize*resolution*...
    scanData.Center{i}(:,2),height)
    hold on h=h-resolution*resize;
    end hold off %ylim([0 4000]);
    %xlim([0  4000]);  title(['Centerlines  Through  Thickness,
    ',suture]) caz = -5; cel = 30;
    view([caz,cel]);
    saveas(fig,[suturesave,'3D_Centerlines.jpg'])


    % Determining the suture length for
    i=1:(length(Data.Files))
    scanData.CenterDistance{i}=diff(scanData.Center{i});
    scanData.CenterDistance{i}=sqrt(scanData.CenterDistance{i
    }(:,1).^2+... scanData.CenterDistance{i}(:,2).^2);
    scanData.SutureLength{i}=sum(scanData.CenterDistance{i});
    end

    % Determining LII (keeping in units of pixels)
    scanData.SumLII=0; for i=1:(length(Data.Files))
    scanData.LinDist{i}=sqrt((scanData.Center{1,i}(end,1)...
    scanData.Center{1,i}(1,1))^2+(scanData.Center{1,i }(end,2)-
        ...
```

75

```matlab
        scanData.Center{1,i}(1,2))^2);
        scanData.LII{i}=scanData.SutureLength{i}/scanData.
    LinDist{i};
     scanData.SumLII=scanData.SumLII+scanData.LII{i};
end
% Mean   LII   of   Dataset   for   i=1:(length(Data.Files))
scanData.MeanLII{i}=scanData.SumLII/length(Data.Files)
      ; end

% Plotting   LII   vs   Height   fig=figure;
scatter([scanData.LII{:}],  [scanData.h_LII{:}],  'filled')
hold  on  plot([scanData.MeanLII{:}],  [scanData.h_LII{:}],
'r', '
  LineWidth', 1); hold off title(['Suture LII Through Skull
Thickness, ',suture]) xlabel('Linear Interdigitation Index')
ylabel('Position in Skull, \mum (Datum at inner surface)')
%ylim([0 500]); %xlim([1 3]); legend('LII at
Slice','Average LII of Suture')
saveas(fig,[suturesave,'LII_Thickness.jpg'])

% Determining   Average   Width   of   Each   Slice
scanData.SumWidth=0;      for      i=1:(length(Data.Files))
scanData.AvgWidth{i}=resize*resolution.*sum(scanData.Width
{i})/...
    length(scanData.Width{i});
    scanData.SumWidth=scanData.SumWidth+scanData.AvgWidth{
    i};
end
% Mean Average Width of Dataset for i=1:(length(Data.Files))
scanData.MeanWidth{i}=scanData.SumWidth/length(Data.
      Files); end
```

76

```matlab
% Plotting Average Width vs. Height fig=figure;
scatter([scanData.AvgWidth{:}], [scanData.h_LII{:}], '
filled') hold on
plot([scanData.MeanWidth{:}], [scanData.h_LII{:}], 'r', '
   LineWidth', 1); hold off title(['Suture Average Width
Through Thickness, ',suture]) xlabel('Average Width, \mum')
ylabel('Position in Skull, \mum (Datum at inner surface)')
%ylim([0 500]); %xlim([100 400]); legend('Average Width at
Slice','Average Width of Suture')

% Above used to display value
saveas(fig,[suturesave,'Width_Thickness.jpg'])

%   Saving   Data   save('scanData.mat','scanData')   for
i=1:(length(scanData.LII))
    LII(i) = scanData.LII{i};
    SutureLength(i) = scanData.SutureLength{i};
    AvgWidth(i) = scanData.AvgWidth{i};
    LinDist(i) = scanData.LinDist{i}; end
xlswrite('TestResults.xlsx',LII,1,'B1')
xlswrite('TestResults.xlsx',SutureLength,1,'B2')
xlswrite('TestResults.xlsx',AvgWidth,1,'B3')
xlswrite('TestResults.xlsx',LinDist,1,'B4')
```

C.3 Suture Width Analysis

This code identifies the boundaries of the suture, determines the center line through skeletonization, and analyses the suture at every point in the center line.

```matlab
function [Center,Width] = SutureAnalysisMAClosestDist(
   LoadedImage,ID)
%% Tracing boundary starting from top left corner of the
   suture and finding
```

```matlab
% top and bottom curves of the suture using corner points
TempFig=figure;        imshow(LoadedImage);        set(gcf,
'units','normalized','outerposition',[0 0 1 1]); % Maximize
figure.
TempPos = get(gca,"InnerPosition"); notice = questdlg('Scale
and shift the image so you can select top left corner of the
suture ','Prepare the image','Yes','Yes');
pause; title('Select a point at the top left corner of the
suture
   '); hold on; questdlg('Select a point at the top left
corner of the suture','Point selection','Yes','Yes');
[xi,yi] = getpts; close(TempFig);

TempFig=figure;        imshow(LoadedImage);        set(gcf,
'units','normalized','outerposition',[0 0 1 1]); % Maximize
figure. hold on;


notice = questdlg('Select 3 points along the suture edge
     with following order: TopRight, BottomRight, BottomLeft
  ','Point selection','Yes','Yes');
[xi2,yi2] = getpts; close(TempFig); xi=[xi;xi2];
yi=[yi;yi2];

%        Tracing        boundary        contour        =
bwtraceboundary(LoadedImage,[round(yi(1)),        round
(xi(1))],'E',8);
TopLeft = 1;
[~, TopRight] = ClosestPoint([yi(2),xi(2)],contour);
[~, BottomRight] = ClosestPoint([yi(3),xi(3)],contour);
[~, BottomLeft] = ClosestPoint([yi(4),xi(4)],contour);
```

78

78

```matlab
%Splitting into top and bottom curves
Top = flip(contour(TopLeft:TopRight,:),2);
Bottom = flip(flip(contour(BottomRight:BottomLeft,:),1),2)
    ;

% Smoothing the top and bottom curves
NormLength = length(Bottom); %Normalization of the number
    of points. Using bottom curve as a base
TopS(:,1)=smooth(smooth(smooth(TimeNorm(Top(:,1),
    NormLength))));
TopS(:,2)=smooth(smooth(smooth(TimeNorm(Top(:,2),
    NormLength))));
    BottomS(:,1)=smooth(smooth(smooth(TimeNorm(Bottom(:,1),
    NormLength))));
BottomS(:,2)=smooth(smooth(smooth(TimeNorm(Bottom(:,2),
    NormLength))));

SuturePlot = figure();
line(Top(:,1),Top(:,2),'Color','g','LineWidth',2); hold on;
line(Bottom(:,1),Bottom(:,2),'Color','c','LineWidth',2);
xlabel('X [pixels]'); ylabel('Y [pixels]'); axis ij; axis
tight; axis equal; hold off;

%% ------ Skeletonization to find the Medial Axis (ME)
    --------------------
MinLength = 50; % Minimum Length of the Branch in the pruning
process. Loaded = bwskel(LoadedImage); figure; imshow(Loaded)
LoadedImageSkeleton = bwmorph(bwskel(LoadedImage,'
    MinBranchLength',MinLength),'spur'); figure;
imshow(LoadedImageSkeleton)
LoadedImageSkeleton1 = bwmorph(bwskel(bwskel(
```

```matlab
    LoadedImageSkeleton,'MinBranchLength',MinLength)),'spur
    '); figure;
imshow(LoadedImageSkeleton1)
LoadedImageSkeletonNoPrune = bwmorph(bwskel(LoadedImage),'
    spur');
TempFig=figure; imshow(LoadedImageSkeleton);
[SkelY, SkelX]=find(LoadedImageSkeleton);

notice = questdlg('Scale and shift the image so you can
    select left end of the suture ','Prepare the image','
    Yes','Yes'); pause;
[xi3,yi3] = getpts; close(TempFig);
SkelStroke = points2stroke([SkelX,SkelY],xi3,yi3);
% line(SkelStroke(:,1),SkelStroke(:,2));
SkeletonS(:,1) = smooth(SkelStroke(:,1));
SkeletonS(:,2) = smooth(SkelStroke(:,2));
line(SkeletonS(:,1),SkeletonS(:,2),'Color','r');

figure(SuturePlot); hold on;
line(TopS(:,1),TopS(:,2),'Color','#006400');
line(BottomS(:,1),BottomS(:,2),'Color','b');
% line(SkeletonS(:,1),SkeletonS(:,2),'Color','k','
    LineStyle','none','Marker','.'); text(100,100,'Top and
Bottom curves of the suture with the
    MA created by skeletonization'); hold off;

Center=SkeletonS; % returning SkelStroke as a center (
    Medial Axis)

%% -----Taking measurements by finding the closest distance
    between -------
```

```matlab
% ------------top and bottom curve through every point of
   MA -------------

% Putting search parameters astep=1; %Angular step size
along search span aspan=90; %Angular search span. -Span to
+Span with an step equal to astep
vlength=50; %length of the vector to spreading from the
   center point
A=[]; % Angle between consecutive width measurements
T=zeros(size(Center));
B=zeros(size(Center));
Width=NaN(length(Center),1);

Rot=@(a)[cosd(a) -sind(a); sind(a) cosd(a)];

tic
for i=1:length(Center)
    % Finding normal to the center line as a initial vector
       to start search
    if i == length(Center)
        V = (Rot(-90)*vlength*((Center(i,:)-Center(i-1,:))
         /norm(Center(i,:)-Center(i-1,:)))')'; else
       V = (Rot(-90)*vlength*((Center(i+1,:)-Center(i,:))
         /norm(Center(i+1,:)-Center(i,:)))')'; end

%     line([Center(i,1)-V(1,1),Center(i,1)+V(1,1)],[Center
   (i,2)-V(1,2),Center(i,2)+V(1,2)],'Color','y');


    % Creating NaN matrix for storege of intersection
       points of rotated
    % vectors with top and bottom curves
```

```matlab
Tnew = NaN(2*aspan/astep+1,2);
Bnew = NaN(2*aspan/astep+1,2);


for j=-aspan:astep:aspan
    VRot=(Rot(j)*V')'; %Rotating the normal vector to
        find the closest distance
    VSearch = [Center(i,:)-VRot;Center(i,:)+VRot];
    % Detectng intersection with top curve
    [X1,Y1,~]=polyxpoly(VSearch(:,1),VSearch(:,2),TopS
        (:,1),TopS(:,2)); if length(X1)==1
          Tnew(j+aspan+1,:)=[X1,Y1]; elseif length(X1)>1
            [Tnew(j+aspan+1,:),~]=ClosestPoint(Center(i,:)
             ,[X1,Y1]); end

    % Detectng intersection with bottom curve
    [X2,Y2,~]=polyxpoly(VSearch(:,1),VSearch(:,2),
        BottomS(:,1),BottomS(:,2)); if length(X2)==1
          Bnew(j+aspan+1,:)=[X2,Y2]; elseif length(X2)>1
            [Bnew(j+aspan+1,:),~]=ClosestPoint(Center(i,:)
             ,[X2,Y2]); end
end
CT=Tnew-repmat(Center(i,:),length(Tnew),1);
CB=Bnew-repmat(Center(i,:),length(Bnew),1);
LocalWidth=sqrt(CT(:,1).^2+CT(:,2).^2)+sqrt(CB(:,1)
   .^2+CB(:,2).^2);
Index=find(LocalWidth==min(LocalWidth));
T(i,:)=Tnew(Index(1),:);
B(i,:)=Bnew(Index(1),:);
Width(i,:)=LocalWidth(Index(1),:);
```

```matlab
% Filling gaps when here is an angle difference greater
    than 7 degrees
% between 2 consecutive with lines
TB=B(i,:)-T(i,:); % since positive direction of X is down
    wit ij axis, we are calculating the angle based on the
    vector from top 2 bottom

if i==1
    Anew=0;
    Adiff=Anew; else
    V1 = B(i-1,:)-T(i-1,:);
    V2 = B(i,:)-T(i,:);
    Anew = atan2d(det([V1;V2]),dot(V1,V2)); end
A=[A;Anew]; if length(A)>1
    Adiff=Anew; AdiffAbs = abs(Adiff); if AdiffAbs>10
        Adivide=ceil(abs(Adiff/5));
        Cadd=repmat(Center(i-1,:),Adivide-1,1)+repmat
            ((1:Adivide-1)',1,2).*repmat((Center(i,:)-
          Center(i-1,:))/Adivide,Adivide-1,1);
%          line(Cadd(:,1),Cadd(:,2),'Color','k','
LineStyle','none','Marker','o');
        V1=3*(B(i-1,:)-T(i-1,:));

        % Place holders for added points
        Tmid=[];
        Bmid=[]; for j=1:(Adivide-1)
            V1 = (Rot(5*Adiff/abs(Adiff))*(V1)')';

            % Detectng intersection with top curve
            [X1,Y1,~]=polyxpoly([Cadd(j,1),Cadd(j,1)V1(
                1)],[Cadd(j,2),Cadd(j,2)-V1(2)],TopS
```

83

```matlab
              (:,1),TopS(:,2));
if ~isempty(X1) if length(X1)==1
        Tmid(j,1)=X1(1);
        Tmid(j,2)=Y1(1); else
        IntersectDistance=sqrt((X1-Cadd(j
            ,1)).^2+(Y1-Cadd(j,2)).^2);
        IntersectIndex=find(
            IntersectDistance==min(
        IntersectDistance));
        Tmid(j,1)=X1(IntersectIndex);
        Tmid(j,2)=Y1(IntersectIndex); end
else
    Tmid(j,1)=nan;
    Tmid(j,2)=nan; end

% Detecting intersection with bottom curve
[X2,Y2,~]=polyxpoly([Cadd(j,1),Cadd(j,1)+
    V1(1)],[Cadd(j,2),Cadd(j,2)+V1(2)],
    BottomS(:,1),BottomS(:,2));

if ~isempty(X2) if length(X2)==1
        Bmid(j,1)=X2(1);
        Bmid(j,2)=Y2(1); else
        IntersectDistance=sqrt((X2-Cadd(j
            ,1)).^2+(Y2-Cadd(j,2)).^2);
        IntersectIndex=find(
            IntersectDistance==min(
        IntersectDistance));
        Bmid(j,1)=X2(IntersectIndex);
        Bmid(j,2)=Y2(IntersectIndex); end
else
```

```matlab
                            Bmid(j,1)=nan;
                            Bmid(j,2)=nan; end
                        line([Tmid(j,1);Bmid(j,1)],[Tmid(j,2);Bmid
                            (j,2)],'Color','c'); end
                    BTdist=Tmid-Bmid; BTmidpoint=(Tmid+Bmid)/2;
                    WidthAdd=(BTdist(:,1).^2+BTdist(:,2).^2).^0.5;
                    Center=[Center;Cadd];
                    Width=[Width;WidthAdd]; end
        end

%       line(Center(i,1),Center(i,2),'Color','b','LineStyle
    ','none','Marker','.');
    line([T(i,1);B(i,1)],[T(i,2);B(i,2)],'Color','m');
    title(['#',num2str(ID),', Angular step ',num2str(astep
        ),', Angle span ',num2str(-aspan),' ~ ',num2str(
        aspan),', Angle difference ',num2str(Adiff)]);
    if mod(i,200) == 0
                drawnow;
    end
end
[Center, Width] = points2stroke2([Center,Width],Center
    (1,1),Center(1,2));

% Width=[Width;norm(T(end,:)-B(end,:))];
WidthAverage=mean(Width); CenterDistance=diff(Center);
CenterDistance=sqrt(CenterDistance(:,1).^2+CenterDistance
    (:,2).^2);
SutureLength=sum(CenterDistance); Lengths=0;
for j=1:length(CenterDistance)
    Lengths=[Lengths;Lengths(end,1)+CenterDistance(j,1)];
end
```

```matlab
figure();
stem(Lengths,Width,'b','MarkerSize',1); hold on;
plot([0,Lengths(end,1)],[WidthAverage,WidthAverage],'r');
title('Sutural width along the sutural length');
legend('Width of the sutures along the sutural length','
    Average with','Location','NorthWest','Box','off');
xlabel('Sutural length [pixels]'); ylabel('Sutural width
[pixels]'); disp(['Time spent on image #',num2str(ID)]);
toc
```

C.4 Suture Closest Point Measurement

This code finds the closest distance between the top and bottom margins of the suture.

```matlab
function [P,Dist,ii]=ClosestPoint2(Point,Data)
[row,~]=size(Data);
SubVector=Data-repmat(Point,row,1);

Dist=sqrt(SubVector(:,1).^2+SubVector(:,2).^2);
ii=find(Dist==min(Dist)); P=Data(ii,:);
```

C.5 Creating Strokes between Suture Margins

This code creates vectors between the top and bottom margins of the suture that will help find the closest distance to find the suture width.

```matlab
function [Stroke,Extra] = points2stroke2(Data,StartX,
    StartY)
    [row, ~] = size(Data); Stroke = [];
    Extra = []; State = 0; while row >1 if State == 0
SubVector=Data(:,1:2)-repmat([StartX,StartY],row ,1);
        State =1; else
        SubVector=Data(:,1:2)-repmat(Stroke(end,:),row,1);
    end
```

86

```matlab
Distance=sqrt(SubVector(:,1).^2+SubVector(:,2).^2);
[~,ii]=min(Distance);
Stroke = [Stroke;Data(ii,1:2)];
Extra = [Extra;Data(ii,3:end)]; Data(ii,:) = []; row =
row-1;
end
Stroke = [Stroke;Data(:,1:2)]; Extra =
[Extra;Data(:,3:end)];
```

Appendix D: Sample Morphological Data

This section is a summary of all the morphological data; suture width and LII, obtained from the 42 samples across 9 maxillae.

Table 6: Suture Width and LII Data

Swine #	Sample #	Suture Width (μm)			Suture LII		
		Min	Max	Mean	Min	Max	Mean
9	1	196.7546	215.8924	203.3452	2.791788	3.210738	2.990114
	2	183.1082	206.4282	196.382	3.345646	4.011237	3.566657
	3	177.5998	199.2781	185.2346	3.82493	4.174755	3.997942
	4	197.9724	219.0853	206.6698	3.21798	3.575391	3.40401
10	1	199.7996	228.7997	213.656	1.906976	2.146485	1.986803
	2	208.4715	263.0233	227.633	1.849701	2.013205	1.94152
	3	197.5944	230.4364	205.9522	2.233012	2.506921	2.369813
	4	196.3256	224.5341	206.4497	2.638267	2.937981	2.737719
	5	194.1787	228.2132	211.9055	2.877413	3.130063	2.944972
11	1	214.9885	227.3647	221.3559	2.783623	3.037456	2.93297
	2	216.5007	242.7026	231.997	2.683511	3.42908	2.917728
	3	186.6982	215.3365	200.987	3.529415	4.184226	3.824013
	4	207.0988	225.2759	215.6132	3.300572	3.784627	3.571783
	5	224.7286	248.9455	235.0744	2.8398	3.2362	3.053636

		Suture Width (µm)			Suture LII		
Swine #	Sample #	Min	Max	Mean	Min	Max	Mean
12	1	271.3445	310.0713	293.6651	2.034096	2.241603	2.106518
	2	286.7095	326.4382	298.1222	1.965643	2.166394	2.061715
	3	253.8892	268.6077	263.0731	2.26033	2.807165	2.576228
	4	241.9695	260.556	252.071	2.870932	3.20349	2.97294
15	5	234.267	257.6225	243.0362	3.008515	3.317726	3.165001
	2	237.8375	254.5518	246.8989	2.340424	2.636129	2.455042
	3	218.3229	245.7322	228.2556	2.261228	2.606255	2.461602
	4	218.9351	229.9884	224.1913	2.387217	2.732546	2.614102
16	1	259.8246	287.5712	269.681	1.671618	1.833979	1.764511
	2	228.0438	251.7818	239.3809	1.908357	2.257055	2.120888
	3	214.9867	238.0751	225.4609	2.265747	2.533604	2.425694
	4	199.797	216.5093	209.3103	2.531519	2.783651	2.66011
	5	212.8569	226.8587	219.3535	2.802952	3.087475	2.939324
17	1	188.2137	213.1796	202.4004	2.158023	2.390408	2.277571
	2	194.9287	219.2859	206.7495	2.216577	2.449398	2.322607
	3	208.0824	215.371	212.7874	2.363106	2.765616	2.522887
	4	203.7949	220.8942	211.2076	3.035267	3.359803	3.154112
	5	197.3447	219.4374	207.9583	2.901453	3.28086	3.082897